



1 Upper stratospheric ClO and HOCl trends (2005–2020): Aura 2 Microwave Limb Sounder and model results

3 Lucien Froidevaux¹, Douglas E. Kinnison², Michelle L. Santee¹, Luis F. Millán¹, Nathaniel J. Livesey¹,
4 William G. Read¹, Charles G. Bardeen², John J. Orlando², and Ryan A. Fuller¹

5
6 ¹Jet Propulsion Laboratory, California Institute of Technology, Pasadena, California, USA

7 ²National Center for Atmospheric Research, Boulder, Colorado, USA

8 *Correspondence to:* Lucien Froidevaux (lucienf@jpl.nasa.gov)

9 **Abstract.** We analyze Aura Microwave Limb Sounder (MLS) monthly zonal mean time series of ClO and HOCl
10 between 50°S and 50°N to estimate upper stratospheric trends in these chlorine species from 2005 through 2020.
11 We compare these observations to those from the Whole Atmosphere Community Climate Model version 6
12 (WACCM6), run under the specified dynamics configuration. The model sampling follows the MLS coverage in
13 space and local time. We use version 5 MLS ClO zonal mean daytime profiles and similarly binned daytime ClO
14 model profiles from 32 to 1.5 hPa. For MLS HOCl, we use the version 5 offline product derived from daily zonal
15 mean radiances rather than averaged Level 2 profiles; MLS HOCl is scientifically useful between 10 and 2 hPa,
16 and the HOCl monthly zonal means are separated into day and night for comparison to WACCM6. We find good
17 agreement (mostly within ~10%) between the climatological MLS ClO daytime distributions and the model ClO
18 climatology for 2005–2020. The model HOCl climatology, however, underestimates the MLS HOCl climatology
19 by about 30%. This could well be caused by a combination of fairly large systematic uncertainties in both the
20 model-assumed rate constant for the formation of HOCl and the MLS HOCl retrievals themselves.

21 The model daytime ClO trends versus latitude and pressure agree quite well with those from MLS. MLS-
22 derived near-global upper stratospheric daytime trends between 7 and 2 hPa are -0.73 ± 0.40 %yr⁻¹ for ClO and $-$
23 0.39 ± 0.35 %yr⁻¹ for HOCl, with 2σ uncertainty estimates used here. The corresponding model decreases are
24 somewhat faster than observed (although the difference is not statistically significant), with trend values of
25 -0.85 ± 0.45 %yr⁻¹ for ClO and -0.64 ± 0.37 %yr⁻¹ for HOCl. Both data and model results point to a faster trend
26 in ClO than in HOCl. The MLS ClO trends are consistent with past estimates of upper stratospheric ClO trends
27 from satellite and ground-based microwave data. As discussed in the past, trends in other species (in particular,
28 positive trends in CH₄ and H₂O) can lead to a ClO decrease that is faster than the decrease in total inorganic



29 chlorine. Regarding trends in HOCl, positive trends in HO₂ can lead to a faster rate of formation for HOCl as a
30 function of time, which partially offsets the decreasing trend in active chlorine.

31 The decreasing trends in upper stratospheric ClO and HOCl provide additional confirmation of the
32 effectiveness of the Montreal Protocol and its amendments, which have led to the early stages of an expected
33 long-term ozone recovery from the effects of ozone-depleting substances.

34 **1 Introduction**

35 Changes in the gaseous chlorine content of the atmosphere have been scrutinized since the late 1970s, when
36 prescient warnings (Molina and Rowland, 1974) were made regarding likely threats to the Earth's stratospheric
37 ozone (O₃) layer from the decomposition of various chlorofluorocarbons (CFCs) emitted at the surface by human
38 industrial activities. These threats carried human health implications as a result of increased ultraviolet (UV)
39 radiation at the surface, which would follow from reductions in UV absorption by stratospheric ozone. Various
40 measurements of the abundances of different chlorine species in the stratosphere followed these early years of
41 concern regarding expected declines in global ozone. Early balloon-borne observations of chlorine monoxide
42 (ClO) radicals in the upper stratosphere (Anderson et al., 1977; Waters et al., 1981) confirmed the predicted
43 importance of gas-phase reactions (involving ClO, Cl, O₃, and O) on upper stratospheric ozone abundances. Since
44 the 1987 Montreal Protocol and its subsequent amendments, established to strongly reduce worldwide surface
45 emissions of halogenated compounds harmful to the ozone layer, both the tropospheric and stratospheric chlorine
46 budgets have been carefully studied and monitored by the atmospheric science community. This was motivated
47 by enhanced concerns regarding ozone decreases in the lower stratosphere, after the discovery of the seasonal
48 appearance of an ozone hole over Antarctica (Farman et al., 1985).

49 Studies of interannual and longer-term changes in stratospheric chlorine species were carried out by ground-
50 based (column) measurements of HCl and ClONO₂ at infrared wavelengths (Rinsland et al., 2003; Kohlhepp et
51 al., 2011; Mahieu et al., 2014). Near-global stratospheric chlorine changes have also been tracked by satellite
52 measurements of HCl. Indeed, this chlorine reservoir species at high altitude (near 50 km) accounts for the vast
53 majority of Cl_y (total inorganic chlorine), based on past measurements of the stratospheric chlorine budget by
54 Zander et al. (1992) and Nassar et al. (2006). Froidevaux et al. (2006) also discussed model results regarding the
55 contribution of upper stratospheric HCl to Cl_y and described measurable decreases in HCl (and by inference, in
56 Cl_y) from mid-2004 to early 2006, based on changes in Aura MLS profiles. The rather fast rise in chlorine from
57 the 1980s to the late 1990s (with increases of more than 55%) was followed by a slower rate of decrease, as



58 expected from model calculations. Stratospheric chlorine follows the overall tropospheric trends with about a 5-
59 year delay, which accounts for transport and mixing of tropospheric compounds into the stratosphere (as discussed
60 by Anderson et al., 2000, Waugh et al., 2001, and others).

61 Changes in chlorine source gases at the surface, as well as changes in stratospheric chlorine species, have been
62 updated and documented regularly in quadrennial reports (see WMO, 2018). Based on such analyses, stratospheric
63 HCl has been decreasing over the past two decades by about 0.5–1%yr⁻¹. This includes results from ground-based
64 infrared measurements, as well as from near-global upper stratospheric HCl measurements by the Atmospheric
65 Chemistry Experiment Fourier Transform Spectrometer (ACE-FTS) (see Bernath and Fernando, 2018). These
66 results are consistent with surface total chlorine trends, based on in situ sampling of a large number of source
67 species by ground-based networks (Engel and Rigby et al., 2018), so that there is a good corroboration of the
68 effectiveness of the Montreal Protocol and its amendments, except for some recent departures from expectations
69 for the evolution of CFC-11 (Montzka et al., 2018). Ground-based microwave measurements of stratospheric ClO
70 profiles over the past two decades have also made valuable contributions to these long-term chlorine composition
71 records. This includes trend results for upper stratospheric ClO over Hawaii (Solomon et al., 2006; Connor et al.,
72 2013) as well as for the more variable lower stratosphere over Antarctica (Nedoluha et al., 2016). These findings
73 corroborate the longer-term decreasing trends in HCl (and Cl_y), although dynamical variability on timescales of
74 5–7 years complicates trend detection (e.g., for HCl) in the lower stratosphere (Mahieu et al., 2014; Strahan et al.,
75 2020); this variability and its causes are still under investigation in the community.

76 Here, we provide an analysis of upper stratospheric trends in near-global ClO and hypochlorous acid (HOCl).
77 These two chlorine species have been measured by the Aura Microwave Limb Sounder (MLS) globally on a near-
78 daily basis since its launch in 2004. An analysis of their trends falls within the general theme of confirming that
79 the Montreal Protocol has been able to significantly reduce the threat of stratospheric chlorine to global ozone.
80 The MLS measurements of upper stratospheric ClO and HOCl have taken on a larger role, in light of the fact that
81 MLS lost the capability of obtaining trend-quality data on upper stratospheric HCl after a hardware issue in early
82 2006 (see Livesey et al., 2020). The lower stratospheric HCl measurements have continued through the use of
83 radiances from an adjacent MLS measurement band (see also the lower stratospheric MLS HCl comparisons to
84 model results by Froidevaux et al., 2019). In Section 2, we describe the observations, model simulations, and
85 methods of analysis for this work. Section 3 focuses on the trend results for ClO and HOCl, while Section 4
86 provides a discussion in the context of broader trends in upper stratospheric species. Our conclusions are
87 summarized in Section 5.



88 **2 Observations, model simulations, and analysis methods**

89 In this work, we analyze temporal changes in upper stratospheric ClO and HOCl abundances, based on continuous
90 MLS observations of both species from 2005 through 2020. We compare these observational results to those from
91 a state-of-the-art chemistry climate model for the same time period.

92 **2.1 Observations**

93 The primary datasets used in this analysis come from 16 full years (2005 through 2020) of global measurements
94 performed by Aura MLS. The MLS antenna scans the atmospheric limb as the Aura satellite orbits the Earth in a
95 near-polar sun-synchronous orbit; the instrument measures thermal emission (day and night), using microwave
96 radiometers operating at frequencies near 118, 190, 240, and 640 GHz, as well as a 2.5 THz module to measure
97 OH (during the early part of the mission only). MLS has been providing a variety of daily vertical stratospheric
98 temperature and composition profiles (~3500 profiles per day per product), with some measurements extending
99 down to the upper tropospheric region, and some into the upper mesosphere or higher. We rely here mainly on
100 the upper stratospheric MLS measurements of ClO and HOCl, obtained from 640-GHz radiometer data.
101 Specifically, ClO and HOCl emissions are obtained from lines centered at 649.5 and 635.9 GHz, respectively;
102 Waters et al. (2006) have provided an overview of the MLS instrument and its measurements, along with some
103 sample spectra, and Read et al. (2006) have described the simulated forward model and related spectra. The MLS
104 retrievals use an optimal estimation approach (Rodgers, 2000), with MLS-specific details provided by Livesey et
105 al. (2006); there is no assumption of atmospheric homogeneity along the line of sight (see Livesey and Read,
106 2000), and the MLS retrievals make use of the instrument's views (which are all along the line of sight) during
107 multiple consecutive MLS antenna scans of the Earth's limb. Data users interested in MLS data quality and
108 characterization, estimated errors, and related information, should consult Livesey et al. (2020), the latest update
109 to the MLS data quality document.

110 In this work, we use the latest data version from MLS, namely version 5.0 (or v5). The single-profile precision
111 (1σ random uncertainty) is ~0.1 ppbv for the ClO retrievals in the region between 32 and 1.5 hPa that we focus
112 on here; the vertical resolution of the ClO measurements is about 3–4 km. For our analyses of daytime MLS ClO
113 monthly zonal means in 5° latitude bins, the more relevant precision for averaged upper stratospheric values drops
114 to about 0.5–5%. In addition, the methodology used by the MLS team to assess the aggregate effects of simulated
115 errors in various input parameters on the measurement retrievals (see Livesey et al., 2020) leads to systematic
116 uncertainties of order 0.02–0.1 ppbv for upper stratospheric ClO, which translates to about 5–100% for ClO,



117 depending on whether one considers the peaks of the distributions (for the smaller uncertainty values) or regions
118 away from these peaks. The standard MLS data quality screening methodology (see the above reference) has been
119 applied to all Level 2 ClO profiles, prior to averaging into monthly zonal means.

120 For the MLS HOCl data, we have used an offline retrieval product that shows similar results as the averaged
121 Level 2 profiles, but with somewhat smaller variability. This product is created offline (i.e., after the daily
122 processing of incoming MLS data) by averaging daily Level 1 spectra before performing the retrievals of mean
123 daily profiles, which are then averaged for this work into either day or night monthly zonal means. The offline
124 retrieval technique follows the overall MLS retrieval methodology described by Livesey et al. (2006), except it is
125 a one-dimensional type of retrieval (as it is not used for line-of-sight ‘chunks’ of profiles like the Level 2
126 ‘tomographic’ approach). Moreover, the radiances that are used as part of the averages correspond to profiles for
127 which the temperature and ozone retrievals in Level 2 have passed the standard retrieval criteria for good quality
128 data. This methodology is the same as that used for the MLS offline retrievals of BrO and HO₂, which are also
129 considered to be MLS “noisy products”, based on their single-profile precision values (see Millán et al., 2012,
130 2015, for BrO and HO₂, respectively). These averaged offline products can be more stable and scientifically useful
131 over a wider vertical range than averages of the MLS Level 2 standard products (although the wider vertical range
132 only holds for HO₂). Also, the latitude grid spacing for the MLS offline HOCl product (as for the other offline
133 products mentioned above) is 10°, rather than the 5° used for ClO and other standard MLS retrieval products. We
134 have used the precision and accuracy HOCl estimates from the standard Level 2 MLS product, as we expect
135 similar uncertainties (or possibly better) for the offline HOCl product. The MLS HOCl precision for (day or night)
136 10° monthly zonal means is typically less than 5–10 pptv (or roughly 5–20%). Systematic uncertainties are
137 estimated to be 40–80 pptv for HOCl, or about 25–100%. The more limited useful vertical range for MLS HOCl
138 is 10 to 2 hPa, and the HOCl profiles have a vertical resolution of only 5–6 km.

139 We also make use of upper stratospheric data from ACE-FTS, which was launched in 2003 as part of the
140 Canadian SCISAT mission. The instrument uses the solar occultation technique and gathers measurements in the
141 infrared region (at 750–4400 cm⁻¹, with a spectral resolution of 0.02 cm⁻¹). The ACE-FTS sampling is skewed
142 towards middle to high latitudes, with many fewer profiles per day (per species) than obtained from MLS (30
143 from ACE-FTS versus ~3500 from MLS). ACE-FTS has provided a wealth of constituent profile measurements
144 over basically the same period as Aura MLS (see the overview by Bernath et al., 2017); we use some ACE-FTS
145 trend results to obtain a broader description and understanding of chlorine species trends in the upper stratosphere.
146 We have used ACE-FTS data version 4.1 in the analyses presented here; see Boone et al. (2020) and references
147 therein for detailed information on the ACE-FTS retrievals. We have removed the largest outliers in the ACE-



148 FTS data by using the prescription regarding data flags from Sheese et al. (2019), although this data screening
149 makes essentially no difference to the near-global upper stratospheric data averages and related trend results in
150 this work.

151 2.2 Model simulations

152 The model used here is the Whole Atmosphere Community Climate Model version 6 (WACCM6), a
153 component of the Community Earth System Model 2 (CESM2), configured to use specified dynamics as described
154 by Gettelman et al. (2019). These authors showed that this chemistry climate model reproduces many modes of
155 variability, as well as trends, in the middle atmosphere. WACCM6 is the “high-top” version of the Community
156 Atmosphere Model, version 6 (CAM6; Danabasoglu et al., 2019). CAM6 includes updated representations of
157 boundary layer processes, shallow convection, liquid cloud macrophysics, and two-moment cloud microphysics
158 with prognostic cloud mass and concentration. This version of CAM6 uses a finite volume dynamical core (Lin,
159 2004). The horizontal resolution is 0.95° latitude x 1.25° longitude. The model has 88 levels with a vertical range
160 from the surface to the lower thermosphere. The vertical resolution in the lower stratosphere ranges from 1.2 km
161 near the tropopause to ~ 2 km near the stratopause.

162 The WACCM6 model represents chemical processes from the troposphere into the lower thermosphere. The
163 chemical scheme includes the O_x , NO_x , HO_x , ClO_x , and BrO_x chemical families, along with CH_4 and its
164 degradation products. This scheme also includes primary non-methane hydrocarbons and related oxygenated
165 organic compounds. The chemical processes have evolved from previous versions and are summarized in detail
166 by Emmons et al. (2020). Reaction rates follow the JPL 2015 recommendations (Burkholder et al., 2015). The
167 chemical scheme also includes a new detailed representation of secondary organic aerosols (SOAs), based on the
168 “simple Volatility Basis Set” approach (Tilmes et al., 2019). WACCM includes a total of 231 species and 583
169 chemical reactions broken down into 150 photolysis reactions, 403 gas-phase reactions, 13 tropospheric, and 17
170 stratospheric heterogeneous reactions. The photolytic reactions are based on both inline chemical modules and a
171 lookup table approach (Kinnison et al., 2007).

172 The model scenario used here is based on historical forcings (and recent updates) from the Climate Model
173 Intercomparison Project – Phase 6 (Meinshausen et al., 2017). These include greenhouse gases (CH_4 , N_2O , and
174 CO_2) and organic halogens (CH_3Cl , CH_3CCl_3 , CCl_4 , CFC-11, CFC-12, CFC-113, CFC-114, CFC-115, HCFC-22,
175 HCFC-141b, HCFC-142b, CH_3Br , halon-1211, halon-1301, halon-2402, $CHBr_3$, and CH_2Br_2). CMIP6
176 specification of NO_x emissions from medium energy electrons (MEEs), solar proton events (SPEs), and galactic
177 cosmic rays (GCRs) is also included. The 11-year solar cycle variability is taken from the Naval Research



178 Laboratory's (NRL) solar variability model, referred to as the NRL Solar Spectral Irradiance version 2 (NRLSSI2;
179 Coddington et al., 2016). The volcanic SO₂ emissions (used in the sulfate aerosol density calculation) are derived
180 for each volcanic eruption using the Neely and Schmidt (2016) database updated through the year 2020. This work
181 uses the specified dynamics (SD) option (Lamarque et al., 2012), where reanalysis temperature, zonal and
182 meridional winds, surface stress, surface pressure, and surface latent and sensible heat are used to nudge the model
183 state, thus affecting parameterizations controlling boundary layer exchanges, advective and convective transport,
184 and the hydrological cycle. This model's dynamical constraints, including the Quasi-Biennial Oscillation (QBO),
185 arise from meteorological fields provided by the Modern-Era Retrospective analysis for Research and
186 Applications Version 2 (MERRA-2; Gelaro et al., 2017), and the nudging approach is described by Kunz et al.
187 (2011). The model meteorological fields are nudged from the surface to 50 km; above 60 km, these fields are fully
188 interactive, with a linear transition in between. The model nudging time constant is 50 hours. Model results are
189 obtained from a simulation that, originally, started in 1980 and ended in 2014 (Gettelman et al., 2019); it was later
190 augmented with runs through 2020. After 2014, the greenhouse gas and organic halogen inputs follow the CMIP6
191 SSP2-45 scenario (O'Neill et al., 2016; Riahi et al., 2017), the SPEs are derived from the Geostationary
192 Observational Environmental Satellites (GOES) proton fluxes (Jackman et al., 2008), and the MEEs and GCRs
193 are based on the CMIP6 pre-industrial control.

194 In terms of sampling, the flexibility of WACCM allows for a choice of profiles for local time and spatial
195 coincidences as close as possible to each MLS profile, using the roughly 1° × 1° model bin that includes a given
196 data location for a model local time that falls within 15 minutes of the MLS local time, and binned according to
197 day or night criteria. The model's daily zonal mean profiles (sampled following the MLS locations and local
198 times) are interpolated (as a function of $\log(p)$, where p is pressure) to the MLS retrieval grid points; for ClO and
199 HOCl, this grid is defined by a stratospheric subset of $p(n) = 1000 \times 10^{-n/6}$, in units of hPa, where n is the pressure
200 level index.

201 **2.3 Analysis methods**

202 We have used solar zenith angles less than 90° or larger than 100° to separate daytime from nighttime values,
203 respectively, for both MLS and model profiles; after this selection, monthly zonal means were created.

204 In terms of trend analyses, we follow the approach for MLS data and model trends discussed by Froidevaux et
205 al. (2019), namely a multivariate linear regression (MLR) method, in order to fit the monthly zonal mean time
206 series from both MLS and the model. We refer the reader to Appendix (A3) of the above reference for more details



207 regarding the regression model, which includes commonly used functional terms, namely a linear trend and a
208 constant term, cosine and sine functions with annual and semi-annual periodicities, as well as functions describing
209 variations arising from the QBO and the El Niño / southern oscillation (ENSO); ENSO plays a large role (in
210 comparison to the QBO) only in the lower stratosphere (e.g., Randel and Thompson, 2011). Here, we also include
211 a fitted component that follows variations in solar radio flux (at 10.7 cm), F10.7, based on the Canadian solar
212 measurements described by Tapping (2013). For the trend uncertainty estimates, as mentioned also by Froidevaux
213 et al. (2019), we use a block bootstrap resampling method (Efron and Tibshirani, 1993), as done by Bourassa et
214 al. (2014), Mahieu et al. (2014), and others, in trend analyses of atmospheric composition. Basically, for every
215 fitted time series from MLS and the model, we analyze many (thousands of) resamplings of the fit residuals, with
216 year-long blocks of values replaced by values from randomly chosen years; (twice the) standard deviations in
217 these random distributions provide (2σ) uncertainty values. Such results are typically very similar to the 95%
218 confidence level (which would be arrived at by using the 2.5 and 97.5 percentile limits of the distributions). We
219 have found that such trend uncertainty calculations generally lead to significantly larger error bars than methods
220 that neglect the autocorrelation of the residuals, and even than some methods that include simple correction factors
221 for this autocorrelation (see more details in a later section).

222 **3 Results**

223 **3.1 ClO**

224 We first provide in Fig. 1 an overview of daytime ClO climatological values for January and July (averages
225 for 2005 through 2020) in the 50°S–50°N latitude region, and a comparison to the model results. As a consequence
226 of the photochemical balance between Cl and ClO radicals in the upper stratosphere, the largest ClO abundances
227 occur at pressure levels near 2 to 3 hPa; in the mid- to lower stratosphere, the availability of reactive chlorine is
228 limited by the conversion of ClO and NO₂ to ClONO₂. The observed ClO daytime distributions during January
229 and July are well reproduced by the model results (top and middle panels in Fig. 1, respectively), with ratios
230 between model and data between 0.9 and 1.1 for most latitudes at pressures less than 10 hPa (bottom panels in
231 Fig. 1); in this region, the systematic uncertainty estimates for MLS ClO are about 0.02 to 0.03 ppbv (see Livesey
232 et al., 2020), or of order 5–10%. Near 20–30 hPa, the model ClO values in the winter hemisphere mid- to high
233 latitudes are lower than observed by ~30%, although there is not much available ClO (in a climatological average
234 sense) in this region, and the systematic uncertainty estimates for MLS ClO are of order 0.1 ppbv, which can be
235 as much as 50–100%. Besides these features (and equally good model/data agreement during other months of the



236 year, not shown), we note that the model reproduces the seasonal changes in the peak ClO abundance patterns,
237 which are tied to other seasonal changes. Indeed, it has been shown in the past that seasonal and longer-term
238 variations in the CH₄ and H₂O distributions play a primary role in the chlorine partitioning between upper
239 stratospheric HCl and ClO (see Solomon and Garcia, 1984; Siskind et al., 1998; Froidevaux et al., 2000).

240 Sample time series for the MLS ClO daytime data are shown in Fig. 2, along with the model series, and
241 regression fits (see Sect. 2) to both data and model series. Residual series are shown in the bottom panel of Fig. 2,
242 for the fits to MLS and to the model, and also for the model fit to MLS data, after taking out the average model
243 bias versus the data. In this latitude/pressure bin (35–40°N/2.2 hPa), there is a slight model underestimate of the
244 observed time series, but the modelled temporal decrease (reflected in the relevant fitted line) follows the slope
245 of the observed tendency fairly closely. The root mean square (rms) residual values for this panel, and in general,
246 are close to 5–7%, although the WACCM time series actually fit the MLS data better than the regression fits do,
247 as the rms residuals for (de-biased) WACCM versus MLS data are typically between 3 and 5%. These ClO results
248 are further quantified in Fig. 3, where we show excellent agreement between the modeled and observed trends
249 versus latitude at different pressures, in terms of the magnitude and morphology. These results demonstrate
250 statistically significant decreasing ClO trends of about –0.5 to –1%yr⁻¹ in the region between about 30 and 1 hPa
251 from 2005 to 2020, with very good agreement between the measurements and the WACCM6 simulations. Fig. 3
252 also shows that there is no significant difference between modelled and measured ClO trends, given the size of
253 the uncertainties (displayed in these plots as 2σ error bars), as obtained from the statistics of block bootstrap
254 resampling of the fitted residuals (see Sect. 2.3). This good agreement between modelled and measured ClO trends
255 can also be viewed in the pressure/latitude contour plots of Fig. 4; the trend differences (model minus data trends)
256 shown in the bottom panel are usually less than 0.1 to 0.2%yr⁻¹. In Fig. 5, we give the near-global (50°S to 50°N)
257 ClO profile trend results, based on our analyses of monthly zonal mean daytime profile time series for this region
258 as a whole. We obtain very similar trend values if we average results from separate latitude bins, or if we
259 deseasonalize time series from different (narrower) latitude bins prior to the regression. However, we feel it is
260 appropriate to apply the regression analysis to the whole 50°S to 50°N region to describe the resulting uncertainties
261 in these near-global trends in a consistent way, and (particularly) to compare overall ClO trends to those in other
262 species, as we do in a subsequent section. We see from Fig. 5 that measured near-global ClO trends are of order
263 –0.7 to –0.8%yr⁻¹ in the 15–1.5 hPa range, with values closer to –1%yr⁻¹ near 20 to 30 hPa. Model ClO trends are
264 typically slightly more negative than observed trends, with an average upper stratospheric value closer to
265 –0.9%yr⁻¹ (for pressures less than about 15 hPa). In summary, we find very good agreement in the derived ClO
266 trends between the model and the MLS data for 2005–2020, and the differences are not statistically significant.



267 3.2 HOCl

268 We now show results for HOCl, using the same approach as for ClO. The MLS HOCl offline product (see
269 Sect. 2.1) yields climatological fields displayed in Fig. 6 for January and July, over the 10 to 2 hPa region, where
270 the MLS HOCl data are deemed to be scientifically useful (see Livesey et al., 2020); this vertical range also holds
271 for the offline product. We observe peak HOCl January (daytime) values of about 160 pptv near 5 hPa at mid- to
272 high latitudes in the Southern Hemisphere, with slightly larger July peak values in the Northern Hemisphere (near
273 45°N). These patterns are also seen in the model HOCl (daytime) distributions, albeit with a shift to smaller
274 abundances; as seen from the model/MLS ratios in the bottom panels of Fig. 6, model HOCl values are typically
275 about 30% smaller than the mean measurements from MLS. This model-measurement difference is also seen in
276 the nighttime HOCl climatology, as shown in the supplementary material (Fig. S1). A small upward shift in the
277 altitude of peak nighttime HOCl abundances is seen in the MLS data, in comparison to the daytime case (Fig. 6),
278 as well as in the model values. Such a diurnal shift in the distribution of HOCl was also noted in the global satellite
279 measurements of HOCl made by the Michelson Interferometer for Passive Atmospheric Sounding (MIPAS)
280 aboard Envisat (von Clarmann et al., 2006; 2012). We note here that the MLS HOCl measurements have fairly
281 large systematic uncertainties (2σ estimated systematic errors of 30–100%, see Livesey et al., 2020), which could
282 thus largely explain the model/data differences. We also note that slightly smoother profiles would be obtained
283 by applying the MLS averaging kernels to the model profiles, since the MLS HOCl vertical resolution is 5–6 km;
284 doing so would lead to an even larger model underestimate of the MLS HOCl profiles.

285 Another consideration to factor into the model uncertainties for HOCl has to do with the uncertainties in the
286 rate constant for HOCl formation ($k_{\text{HO}_2+\text{ClO}}$). While the model used here conforms to the JPL Evaluation 18
287 (Burkholder et al., 2015) rate constant for this reaction, a more recent rate constant determination by Ward and
288 Rowley (2016) leads to significantly faster HOCl formation. Model simulations were performed to compare
289 annual mean HOCl abundances (50°S–50°N) based on these different choices of $k_{\text{HO}_2+\text{ClO}}$, as shown in Fig. 7 (a);
290 the percent differences (in panel (b)) indicate that 25–45% larger HOCl abundances are obtained with the faster
291 rate constant, depending on altitude. The issue of a fairly poorly determined HOCl formation rate constant has
292 persisted for a number of years, affecting comparisons of balloon-borne HOCl profiles and model results
293 (Kovalenko et al., 2007), as well as analyses of MIPAS HOCl observations (von Clarmann et al., 2009; 2012).
294 Kovalenko et al. (2007) pointed out the need for a faster rate constant to improve agreement between modelled
295 and measured HOCl, such as the rate constant measured by Stimpfle et al. (1979), in comparison to the current
296 (at the time) value from the JPL Evaluation of Chemical Kinetics and Photochemical Data (Sander et al., 2006);



297 this position was supported by the MIPAS measurements of HOCl and other species over Antarctica (von
298 Clarmann et al., 2009). Using a temperature of 240 K, appropriate for the region of interest here, in previous
299 temperature-dependent laboratory studies leads to five different rate constant values that have oscillated over time.
300 Specifically, the values from Stimpfle et al. (1979), Nikolaisen et al. (2000), Knight et al. (2000), Hickson et al.
301 (2007), and Ward and Rowley (2016), respectively, yield 11.3, 10.3, 6.6, 8.6, and 12.5 (all in units of 10^{-12} cm³
302 molecule⁻¹ s⁻¹), leading to an average of 9.7 with a (1σ) scatter of 2.1, or a range of about 3, if all five estimates
303 are included. For comparison, the latest JPL Evaluation (Burkholder et al., 2019) gives an HOCl formation rate
304 constant of 8.7×10^{-12} cm³ molecule⁻¹ s⁻¹, although that particular report did not take into account the work from
305 Ward and Rowley (2016). However, making use of the Superconducting Submillimeter-Wave Limb-Emission
306 Sounder (SMILES) HOCl, ClO, and HO₂ data versus time of day, Kuribayashi et al. (2014) obtained a seemingly
307 well-constrained estimate of $k_{\text{HO}_2+\text{ClO}}$ for a limited temperature and pressure range ($7.75 \pm 0.25 \times 10^{-12}$ cm³
308 molecule⁻¹ s⁻¹ at 245 K in the upper stratosphere). This leads to a value of $\sim 8.3 \times 10^{-12}$ at 240 K (as inferred using
309 an average temperature dependence), consistent with, but slightly smaller than, the latest evaluation's
310 recommendation mentioned above. To summarize, we find that the differences between MLS and model values
311 could well stem from a combination of uncertainties in both the MLS data and the model, and it is not possible to
312 definitively attribute the discrepancy to one or the other data set. This discussion does not include other uncertainty
313 sources (e.g., the photochemical loss rate of HOCl), as we believe that they are smaller in magnitude.

314 The MIPAS HOCl measurements were taken at about 10am/pm local time during 2002–2004; the SMILES
315 HOCl data cover the full diurnal cycle, but only for part of 2009–2010. The ACE-FTS solar occultation (i.e.,
316 sunrise/sunset) measurements have recently included retrievals of stratospheric HOCl profiles (up to about
317 38 km), as discussed by Bernath et al. (2021). The various satellite measurements of near-global HOCl
318 distributions are not easily compared, given their different local times and the non-negligible diurnal changes in
319 HOCl (see SPARC, 2017). Upper stratospheric peak HOCl values from ACE-FTS, MIPAS, Aura MLS, and
320 SMILES range from about 150 to 200 pptv, with MIPAS providing the largest values, as summarized by Bernath
321 et al. (2021). Khosravi et al. (2013) provided a more detailed intercomparison of HOCl measurements from
322 MIPAS, SMILES, and MLS in the upper stratosphere, with the help of model simulations of the diurnal cycle
323 (and ClO intercomparisons were also discussed). Good agreement was obtained, overall, versus the expected
324 HOCl diurnal variations, despite the noise in some of the data sets (with SMILES HOCl producing the least noisy
325 data). In SPARC (2017), HOCl monthly zonal mean distributions from MIPAS, SMILES, and MLS were
326 intercompared, albeit not for the same range of years (see also the recent update by Hegglin et al., 2021). Nighttime
327 values were used, as this time period exhibits somewhat smaller changes versus local time than the daytime data.



328 The MLS HOCl data were shown to be on the low side (by 20 to 30%) of both the MIPAS and SMILES results,
329 with the SMILES values lying between the MLS and MIPAS values; a low bias in MLS HOCl was also seen in
330 the comparisons presented by Khosravi et al. (2013). However, those studies used v3 HOCl data from the standard
331 MLS product. Mean differences between v3 HOCl and v5 HOCl are of order 5–10%, with the v5 data on the low
332 side of v3. More to the point, the offline HOCl retrievals yield larger values, by about 25%, than the monthly
333 zonal means from the standard v5 product, as can be seen from a comparison of Fig. 6 for the offline MLS HOCl
334 climatology versus Fig. S2 for the standard MLS HOCl product. The HOCl offline data values are thus about 20%
335 larger than the v3 MLS standard product values, so that much of the MLS low bias versus MIPAS and SMILES
336 is mitigated by using the offline MLS HOCl product. It follows from the above comments that the WACCM6
337 values will also significantly underestimate the HOCl abundances from MIPAS and SMILES. Based on the above
338 references discussing past satellite data intercomparisons for HOCl, the (2σ) systematic uncertainties for non-
339 MLS HOCl data sets are likely larger than 10–15%. The MLS v5 HOCl uncertainties are in the 40–80 pptv range
340 (see Livesey et al., 2020), or at least ~25% (and significantly more in the lower part of the upper stratosphere); it
341 is reasonable to expect that the offline MLS HOCl product will be affected by very similar systematic uncertainties
342 as the MLS standard product. In summary, we cannot expect much better agreement between the various HOCl
343 data sets than the (roughly) 20% level of agreement implied here.

344 Turning to the derived trends in HOCl, these will not be affected much (in units of $\%yr^{-1}$) by mean differences
345 between measured and modeled climatological values. As was done earlier for the ClO time series, we show
346 sample daytime HOCl time series, fits, and residuals in Fig. 8. We observe from such time series that, apart from
347 the absolute value difference between MLS and model HOCl, the measured seasonal cycle is well reproduced by
348 the model; less photochemical destruction of upper stratospheric HOCl during the winter months accounts for the
349 wintertime high values in the region shown (top panel). The residuals in this example (and in general) are larger,
350 by at least a factor of two, than those for ClO, and the correlation coefficients for the fits and for model versus
351 data are poorer, especially when comparing regression fits to the data and (de-biased) model fits to the data; the
352 poorer fits arise because the MLS HOCl data set is noisier (even for monthly zonal means) than is ClO. Thus, in
353 the case of HOCl, the regression fits to the model give the best results, in terms of correlation coefficients between
354 the regression fits to the MLS or model series, as well as for the de-biased model curves in comparison to the data,
355 and regarding root mean square residuals (as derived from data such as the curves in the bottom panel of Fig. 8).
356 The derived trends for HOCl are shown in Fig. S3 as a function of latitude, from 2.2 to 10 hPa. Many of the MLS-
357 derived trends at specific pressures and latitudes are not statistically different from a zero-trend value, while the
358 model-derived trends are typically negative (with values that are more negative than the measured trends) and



359 statistically different from zero. Figure 9 provides a summary of the results for MLS and model HOCl trends, with
360 day and night data shown separately, after multiple regression is applied to the averaged 50°S–50°N time series.
361 For MLS data between 3 and 7 hPa, we obtain statistically significant decreasing near-global HOCl trends, both
362 day and night. These results provide an unambiguous indication of decreasing upper stratospheric trends in HOCl,
363 given that negative trend center values occur at all retrieval levels. There is no statistically significant difference
364 between the nighttime and daytime results for either the MLS data or the model. The average model HOCl trend
365 ($-0.6\% \text{yr}^{-1}$) is more negative than the average MLS result ($-0.4\% \text{yr}^{-1}$), although this is not a statistically significant
366 difference, given the (2σ) error bars shown in Fig. 9, and the fact that the MLS HOCl vertical resolution is about
367 6 km, so there are really only about 3 independent retrieval levels in the pressure range displayed in Fig. 9 (and
368 any error reduction for averaged results over all pressures would be by a factor of $\sqrt{3}$, or 1.7, at best). However,
369 the nighttime model and data trends at 2 hPa agree better than the daytime results, with the nighttime MLS trends
370 exhibiting a more homogeneous behavior versus pressure than the daytime MLS trends. This is likely caused by
371 the larger MLS signal for nighttime HOCl (see the climatological values in Fig. S1 versus the daytime values in
372 Fig. 6); the nighttime MLS trend errors are also smaller than the corresponding daytime errors.

373 We show in Fig. 10 a summary of the trend profiles for ClO and HOCl, both based on daytime results. We
374 mentioned above that the nighttime HOCl results agree well with those from daytime HOCl, and display better
375 agreement versus the model nighttime results at 2 hPa. For ClO, we have also checked that nighttime trends over
376 a limited pressure range (from 1.5 to 3.2 hPa) agree with the daytime trends (not shown), but nighttime ClO values
377 are typically much smaller than those during the day at pressures larger than 4 hPa, where we found that no robust
378 nighttime ClO trends can be obtained from the MLS data. Figure 10 demonstrates that both of these chlorine
379 species have decreased over much of the globe during the past 16 years, with the ClO trends being more negative
380 (by $\sim 0.35\% \text{yr}^{-1}$) than the trends in HOCl, both in the model and the observational results. Limiting results to an
381 average over the uppermost stratosphere (between 2.2 and 6.8 hPa for both species), the (daytime) MLS-derived
382 near-global upper stratospheric trends are $-0.73 \pm 0.40 \% \text{yr}^{-1}$ for ClO and $-0.39 \pm 0.35 \% \text{yr}^{-1}$ for HOCl. The (2σ)
383 error bars here are the root mean square value applicable to this vertical range, with no reduction in error bars for
384 the broader region; we would rather use a somewhat more conservative uncertainty than one that is too
385 “optimistic” (such as an error reduction by a factor of two for ClO, which assumes uncorrelated errors between
386 pressure levels). The corresponding model trends for this vertical range are $-0.85 \pm 0.45 \% \text{yr}^{-1}$ for ClO and -0.64
387 $\pm 0.37 \% \text{yr}^{-1}$ for HOCl. Even if the HOCl trends are not significantly different from the ClO trends at any given
388 level, when averaged, these differences do become more significant.



389 4 Discussion

390 We now review our estimated trends in the context of past results, and we discuss potential reasons for different
391 trends in various chlorine species in the upper stratosphere, including the slower decrease in upper stratospheric
392 HOCl in comparison to the ClO decrease. As a reminder of the relative importance of the main inorganic chlorine
393 species in the upper stratosphere, we display in Fig. 11 the percent contribution to total inorganic chlorine (Cl_y)
394 over the 10 to 1 hPa range, based on the climatological (daytime) model results over $50^{\circ}S$ – $50^{\circ}N$ for the time
395 period analyzed here. The Cl_y abundance includes all species contributions from HCl, ClO, HOCl, and ClONO₂,
396 which are shown in the plot, as well as very minor contributions from Cl, Cl₂, Cl₂O₂, OClO, and BrCl. The “Sum”
397 curve shown on the right side of this figure is just the sum from the four main species whose contributions are
398 plotted; this does not quite equal 100% because of the very small (daytime) relative contributions from the latter
399 five species. HCl is clearly the dominant reservoir in the upper stratosphere, as it makes up about 80 to 95% of
400 total inorganic chlorine in this region (see also Froidevaux et al., 2006), while ClO makes up about 5 to 15% of
401 the total, with minor contributions from ClONO₂ and HOCl, both at the few percent level for most of this region.

402 While published trends in chlorine species can be compared, there will always be some differences in the
403 results, given the different measurement locations, coverage, and time periods being considered. We note that the
404 surface maximum in total chlorine was reached in 1992–1993; following the fast initial decrease in methyl
405 chloroform (CH₃CCl₃), tropospheric chlorine declined at a slower rate (O’Doherty et al., 2004). There is also
406 evidence for slightly slower decreases in the ACE-FTS upper stratospheric HCl time series after about 2010
407 (Bernath and Fernando, 2018; Bernath et al., 2020), in comparison to the rate of decline over the 2004–2010
408 period. In terms of the MLS ClO results discussed here, the upper stratospheric trend (for 2005–2020) of
409 $-0.73 \pm 0.40 \text{ \%yr}^{-1}$ can be compared to other estimated trends in upper stratospheric ClO. Jones et al. (2011)
410 reported upper stratospheric ClO trends of $-0.7 \pm 0.8 \text{ \%yr}^{-1}$ for 2001 through 2008, based on a combination of
411 Odin Sub-Millimetre Radiometer (SMR) and Aura MLS data over the tropics; the estimated uncertainty in this
412 satellite-based ClO trend is quite large, but the trend estimate is consistent with our result covering a longer time
413 period. Solomon et al. (2006) displayed the rise and decline of upper stratospheric ClO abundances in the 1982 to
414 2004 time period, based on microwave ground-based profile data from Hawaii. However, the fairly large ClO
415 trend (-1.5 \%yr^{-1}) initially obtained by these authors for 1995–2004 was superseded by analyses of an improved
416 data set over a longer time period using a new methodology (Connor et al., 2013), which led to a ClO trend
417 estimate (at about 4 hPa) of $-0.65 \pm 0.15 (2\sigma) \text{ \%yr}^{-1}$ over the 1995–2012 period. Thus, we find good consistency



418 between our MLS results and previous trend estimates for ClO, especially given the differences in measurement
419 coverage and time periods considered.

420 For the HOCl trends, we are aware of only one prior result, a recent trend estimate based on ACE-FTS HOCl
421 data by Bernath et al. (2021), who quote a marginally significant trend of -0.23 ± 0.22 (2σ) pptv yr⁻¹, which we
422 translate to about -0.19 ± 0.18 %yr⁻¹, given mean HOCl abundances (of 124 pptv) from their analysis of ACE-
423 FTS data at 30–39 km and 60°S–60°N from 2004–2020. This can be compared to our near-global MLS HOCl
424 trend estimate of -0.39 ± 0.35 %yr⁻¹ for a very similar time period; while these two estimates agree within the
425 fairly large uncertainty estimates, the MLS mean trend value represents twice as rapid a decrease as the mean
426 ACE-FTS trend result. At this time, the cause of these differences is not known, although these measurements are
427 among the more difficult for both instruments, and the two sampling patterns are quite different. We note that the
428 model upper stratospheric HOCl trend is faster (at -0.64 ± 0.37 %yr⁻¹) than the MLS-derived trend, and even
429 faster in comparison to the ACE-FTS result.

430 We now turn to some additional model results as well as other relevant measurements from MLS and ACE-
431 FTS, to discuss upper stratospheric trends in chlorine and related species in a broader context. Figure 12 shows
432 the derived average trends in various upper stratospheric chlorine species based on our regression analyses of
433 measured and modeled time series for monthly zonal means from 50°S to 50°N. The near-global upper
434 stratospheric trend values in Fig. 12 are obtained from trends like those in Fig. 10 for MLS ClO and HOCl, but
435 averaged from 6.8 to 2.2 hPa. Error bars represent typical 2σ estimates, calculated from the root mean square of
436 the 2σ estimates for pressures in the 6.8 to 2.2 hPa range; we prefer to use this more conservative error rather than
437 the standard error in the mean, which will typically be an underestimate, since errors from different pressure levels
438 are not completely uncorrelated. As mentioned earlier, no useful MLS-based estimate of HCl trends in the upper
439 stratosphere could be obtained after the related MLS hardware degradation in early 2006. MLS HCl measurements
440 are still scientifically useful in the lower stratosphere, even for trends (see the related model/data analysis by
441 Froidevaux et al., 2019), and certainly they accurately capture the larger seasonal, interannual, and winter polar
442 vortex HCl variations. To derive the trends based on ACE-FTS data shown in Fig. 12, we have used seasonally
443 averaged time series of v4.1 measurements, a methodology used in previous investigations of ACE-FTS trends to
444 lessen the impacts of that instrument's sampling patterns (e.g., see Bernath and Fernando, 2018). We have applied
445 a simple linear fit to the deseasonalized anomalies from ACE-FTS seasonal means (from 50°S to 50°N), thus
446 using the same type of analysis as in the latter reference. In this approach, the auto-correlation of the residuals is
447 taken into account by following the methodology described by Tiao et al. (1990) and Weatherhead et al. (1998);



448 the auto-correlation is assumed to follow a first-order autoregressive model, and the trend error bars are multiplied
449 by a factor that depends on the autoregressive coefficient. We also point out that it would be more complicated to
450 apply the MLR approach used for the MLS and model time series to the ACE-FTS seasonal data, as the MLR
451 method we have used is based on monthly proxy values. A careful intercomparison of different approaches to
452 estimate error bars in various trends analyses is beyond the scope of this paper, although such an intercomparison
453 would be helpful.

454 We see in Fig. 12 (as was shown in Fig. 10) that the MLS ClO trend is more negative than the MLS HOCl
455 trend; this is also true for the model results in Fig. 12, and the model ClO trend is also more negative than the
456 model Cl_y and HCl trends (with respective values of $-0.66 \pm 0.30 \text{ \%yr}^{-1}$ and $-0.64 \text{ \%} \pm 0.30 \text{ \%yr}^{-1} (2\sigma)$). The
457 faster ClO decrease (versus Cl_y or HCl) seen in Fig. 12 is tied to the dependence of ClO on other species. More
458 specifically, the ClO abundance ($[\text{ClO}]$) is roughly proportional to $[\text{HCl}] [\text{H}_2\text{O}]^{1/2} / [\text{CH}_4]$ (see Froidevaux et al.,
459 2000). The model and observed trends in both H₂O and CH₄ agree well (see the bottom portion of Fig. 12). Here,
460 we have averaged all ACE-FTS (50°S–50°N) trends between 33 and 43 km, based on all sunrise and sunset
461 profiles combined. The MLS v5 H₂O trend of $0.13 \pm 0.15 (2\sigma) \text{ \%yr}^{-1}$ is close to the trend we obtain from ACE-
462 FTS data, at $0.18 \pm 0.15 \text{ \%yr}^{-1}$ (which is in reasonable agreement with the near-global mid-stratospheric H₂O trend
463 of 0.24 \%yr^{-1} provided in the broad overview of ACE-FTS trends by Bernath et al., 2020). Although the MLS v4
464 H₂O data suffered from a drift that led to trends that were too large, this drift has been largely mitigated in the v5
465 H₂O data used here (Livesey et al., 2021). The measured trend in CH₄, also obtained from ACE-FTS data, as well
466 as the model CH₄ trend (in very good agreement with the ACE-FTS trend), are significantly larger than the trends
467 in H₂O; more CH₄ will thus lead, in time, to less chlorine in the form of ClO, which means a faster rate of decrease
468 for ClO. The photochemical balance for HOCl, on the other hand, leads to $[\text{HOCl}]$ being roughly proportional to
469 $k_{\text{HO}_2+\text{ClO}} [\text{ClO}] [\text{HO}_2] / (J_{\text{HOCl}} + k_{\text{HOCl}+\text{OH}} [\text{OH}] + k_{\text{HOCl}+\text{O}} [\text{O}])$, where J_{HOCl} is the photodissociation rate constant for
470 HOCl, and the rate constants indicate which HOCl production or destruction reaction we are referring to. In the
471 mid- to upper stratosphere, the J term clearly dominates (e.g., see Chance et al., 1989, and also, based on our
472 diagnostics for the WACCM run used here), and we would thus expect the trend in HOCl to be less negative than
473 the trend in ClO, given that the HO₂ trend is (slightly) positive (per Fig. 12). The MLS-derived trend for HO₂
474 comes from our analysis of the offline MLS HO₂ product (see Millán et al., 2015). As recommended for this
475 product, we performed our trend analysis using day minus night differences, that is, we constructed such monthly
476 zonal means from the set of day and night daily zonal means; the model and data HO₂ trends agree within the
477 error bars, although the MLS error bar is quite large. The model OH trend also points to a slight positive trend,
478 which likely stems from the increasing trends in H₂O. Algebraically, a percent change in HOCl will be driven by



479 the percent change in ClO added to the percent change in HO₂, so that the decreasing trend in HOCl is slowed,
480 relative to the ClO trend, by the increasing trend in HO₂. Using the modelled HO₂ trend in Fig. 12 (~0.2%yr⁻¹),
481 which is consistent with the observed HO₂ trend, one could expect the HOCl trend to lie ~0.2% closer to zero than
482 the ClO trend; this is consistent (within the error bars) with both the modelled and measured trend differences
483 between HOCl and ClO (these differences are ~0.2% and 0.3%, respectively, for the model and for the
484 measurements).

485 The ClONO₂ trends shown in Fig. 12 are less negative than the ClO trends; this likely stems from the slightly
486 positive trends in NO₂, which can mitigate the extent of the decrease in ClONO₂ (formed from ClO and NO₂). We
487 also note that the differences between the model and ACE-FTS HCl trends are somewhat larger than those between
488 the model and MLS ClO, although the error bars in Fig. 12 indicate that none of these differences are statistically
489 significant. It has been shown that the better sampling from emission-type measurements can provide more
490 reliable trend estimates than in the case of sparser sampling (e.g., from occultation-type data; see Millán et al.,
491 2016). We expect that sampling differences between ACE-FTS and MLS (or the model) contribute part of the
492 trend differences versus MLS (or the model). In this regard, error bars in the ACE-FTS trends are likely to be
493 smaller than the errors that would be obtained from a more fully sampled dataset with less data averaging (and
494 thus, with more spatio-temporal variability).

495 While this is less pertinent to the chlorine species trends, we find it interesting that the N₂O trends in Fig. 12
496 appear to be much larger than the trends in NO and NO₂, two radicals that are the products of N₂O destruction in
497 the upper stratosphere; MLS, ACE-FTS, and the model results all point to upper stratospheric trends slightly larger
498 than 1%yr⁻¹, albeit with comparable 2σ uncertainties. Some of this difference might be caused by the strong
499 latitude dependence of the N₂O trends, coupled with large trend uncertainties in a region with rapidly decreasing
500 abundances with height; the N₂O trends from ACE-FTS at lower altitudes yield small positive values that are
501 more consistent with the NO_x trends shown here, and also with tropospheric N₂O trends (see also Bernath et al.,
502 2020). We note also that the MLS N₂O trends likely constitute lower limits, given that there are some unmitigated
503 negative drifts in the version 5 MLS N₂O time series in the lower stratosphere, even after the improvements versus
504 the v4 data (Livesey et al., 2021). Finally, there are also temperature-related effects that could potentially modify
505 the partitioning of chlorine species over the long-term. However, since the average upper stratospheric
506 temperature decrease over the past 16 years is less than 1K (e.g., Steiner et al., 2020), the temperature dependence
507 issue for this time period should not lead to a significant perturbation of chlorine species trends and chlorine
508 partitioning in this region. For the ClO or HOCl photochemical balance in particular, the strongest temperature-
509 dependence (by far) is from the Cl + CH₄ reaction, but even this would lead to a fairly small (15-30%) perturbation



510 (for the cooling rate implied above) in comparison to the impact of the CH₄ trend, or versus the trends in the
511 chlorine species themselves.

512 We have provided above a few arguments that can help explain some of the differences in upper stratospheric
513 chlorine species trends summarized in Fig. 12. The full chemistry climate model takes all the (modelled) factors
514 into account, both regarding photochemical balance issues and any underlying dynamical factors, such as
515 variations and trends in long-lived tracers that can also impact shorter-lived species.

516 **4 Conclusions**

517 We have analyzed Aura MLS monthly zonal mean time series of ClO and HOCl between 50°S and 50°N to
518 estimate upper stratospheric trends in these chlorine species from 2005 through 2020. We compare these
519 observations to those from a state-of-the-art chemistry climate model, WACCM6, run under the specified
520 dynamics configuration, with MERRA-2 meteorological constraints, and sampled for the same time period; in
521 addition, the model sampling follows the MLS coverage in space and local time. We use version 5 MLS ClO
522 zonal mean (Level 3) daytime profiles (associated with solar zenith angles less than 90°) and, for comparison,
523 similarly binned daytime ClO model profiles. For MLS HOCl, we use the version 5 offline product derived from
524 daily zonal mean radiances (in 10° latitude bins) rather than averaged Level 2 profiles; MLS HOCl is scientifically
525 useful between 10 and 2 hPa, and HOCl monthly zonal means are separated into day and night averages (solar
526 zenith angles greater than 100° for night conditions), for comparison to similarly binned WACCM6 HOCl profiles.

527 We find good agreement (mostly within about 10%) between the climatological MLS daytime ClO
528 distributions and the corresponding model ClO climatology for 2005–2020. The model HOCl climatology,
529 however, underestimates the MLS HOCl climatology by about 30% (for both daytime and nighttime). This
530 discrepancy could well be caused by a combination of fairly large systematic uncertainties in both the model-
531 assumed rate constant for the formation of HOCl and the MLS HOCl retrievals themselves, although we note that
532 these model results would likely also underestimate other satellite measurements of HOCl. The model daytime
533 ClO trends versus latitude and pressure agree well with those from MLS ClO. MLS-derived near-global upper
534 stratospheric daytime trends between 7 and 2 hPa are -0.73 ± 0.40 %yr⁻¹ for ClO and -0.39 ± 0.35 %yr⁻¹ for HOCl,
535 with 2σ uncertainty estimates used here. The corresponding near-global upper stratospheric model trends are
536 -0.85 ± 0.45 %yr⁻¹ for ClO and -0.64 ± 0.37 %yr⁻¹ for HOCl. Both data and model results point to a slower trend
537 for HOCl than for ClO. The MLS trends for ClO are generally consistent with past estimates of upper stratospheric
538 ClO trends, based on a combination of Odin/SMR and MLS data from 2001 to 2008 (Jones et al., 2011), and based



539 on ground-based microwave results from Hawaii for 1995–2012 (Connor et al., 2013). The MLS HOCl trend
540 represents a faster rate of change (by about a factor of two) than the marginally significant trend (-0.19 ± 0.18
541 (2σ) %yr⁻¹) that Bernath et al. (2021) obtained from a recent analysis of ACE-FTS HOCl measurements from
542 2004 to 2020.

543 Our general overview (Fig. 12) shows decreasing near-global trends for all the measured upper stratospheric
544 chlorine species. Differences can arise as a result of the impact of trends in other gases that can affect the slowly
545 varying photochemical equilibrium for different species in this region. Notably, observed and modeled positive
546 trends in CH₄ will tend to steepen the decrease of active chlorine (CIO values) in comparison to trends in HCl or
547 Cl_y. Regarding trends in HOCl, positive trends in HO₂ can lead to a faster rate of formation for HOCl as a function
548 of time, which partially offsets the impact of decreases in CIO (also involved in HOCl production).

549 Lastly, the decreasing trends in upper stratospheric CIO and HOCl that are arrived at in this work provide
550 additional confirmation of the effectiveness of the Montreal Protocol and its amendments, which have led to the
551 early stages of an expected long-term ozone recovery from the effects of ozone-depleting substances (see WMO,
552 2018). Indeed, the known decreases in surface chlorine since the early 1990s, which are faithfully included in the
553 model results, have played a major role in the decreasing trends of CIO and HOCl over the 2005–2020 time period.

554

555

556

557

558 *Data availability.* The link <http://disc.sci.gsfc.nasa.gov/Aura/data-holdings/MLS> provides public access to Aura
559 MLS data used here; for the offline MLS HOCl product, the data are available upon request to Luis Millán
560 (luis.f.millan@jpl.nasa.gov). For the availability of ACE-FTS 4.1 data, see <http://www.ace.uwaterloo.ca/data.php>
561 (registration required at <https://database.scisat.ca/l2signup.php>). For solar flux data, the site
562 ftp://ftp.seismo.nrcan.gc.ca/spaceweather/solar_flux/monthly_averages/solflux_monthly_average.txt was used to
563 obtain monthly means of the Canadian F10.7 solar flux measurements; these series (see
564 <http://www.spaceweather.gc.ca>) were included in our regression fits. MERRA-2 data can be obtained from NASA
565 at https://gmao.gsfc.nasa.gov/reanalysis/MERRA-2/data_access/. Model results shown in this paper are available
566 online at:

567 [https://urldefense.us/v3/https://acomstaff.acom.ucar.edu/dkin/ACP_Froidevaux_2021/;!!PvBDto6Hs4WbVuu7!Yk6MAjKksie5II_GsOQzm_FmoXFSt_0ExPIxMEA6hEUdqF6I4S72h5M3WBjsxoKwX1vZRj9wgz6b\\$.](https://urldefense.us/v3/https://acomstaff.acom.ucar.edu/dkin/ACP_Froidevaux_2021/;!!PvBDto6Hs4WbVuu7!Yk6MAjKksie5II_GsOQzm_FmoXFSt_0ExPIxMEA6hEUdqF6I4S72h5M3WBjsxoKwX1vZRj9wgz6b$.)

569



570 *Author Contributions.* LF prepared this manuscript with contributions from all co-authors. DEK provided inputs
571 for running the necessary model runs, as well as properly averaged and formatted outputs from the model, along
572 with various contributions to the main text and Figures. MLS provided assistance in the validation and generation
573 of the MLS ClO data, along with comments on the manuscript. LFM provided the MLS HOCl offline products
574 and related expertise, along with comments on the manuscript. NJL provided leadership for MLS overall, along
575 with comments regarding the manuscript. WGR provided leadership for the MLS forward model and data
576 retrievals, along with measurement science expertise and related manuscript comments. CGB provided assistance
577 towards obtaining the model runs, as well as comments regarding the model description. JJO provided assistance
578 regarding the available laboratory data on the HOCl formation rate constant and its related uncertainties, along
579 with manuscript comments. RAF provided properly formatted and averaged MLS data sets for the various species
580 analyzed in this work.

581

582 *Competing Interests.* The authors declare that they have no conflict of interest.

583

584 *Acknowledgments.* We are thankful to the whole MLS team (past and present) for their contributions over the
585 years to the MLS instrument, data, processing, and database management; all this has contributed to making this
586 research work possible. We also gratefully acknowledge the work of the whole ACE-FTS team in producing and
587 sharing their updated data sets, as these were used here as part of the discussion and comparisons. F10.7 data
588 collection and dissemination are supported by the National Research Council of Canada, with the participation of
589 Natural Resources Canada and support by the Canadian Space Agency. D.E.K. was funded in part by NASA grant
590 (80NSSC20K0926). WACCM is a component of the CESM, supported by the National Science
591 Foundation (NSF). We would like to acknowledge high-performance computing support from Cheyenne
592 (doi:10.5065/D6RX99HX) provided by NCAR's Computational and Information Systems Laboratory, sponsored
593 by the NSF. Work at the Jet Propulsion Laboratory, California Institute of Technology, was performed under
594 contract with the National Aeronautics and Space Administration (80NM0018D0004). Copyright 2021. All rights
595 reserved.

596

597



598 References

- 599 Anderson, J., Margitan, J. J., and Stedman, D. H.: Atomic Chlorine and the Chlorine Monoxide Radical in the
600 Stratosphere: Three in situ Observations, *Science*, 198(4316):501-3, doi:10.1126/science.198.4316.501, 1977.
- 601 Anderson, J., Russell III, J. M., Solomon, S., and Deaver, L. E.: Halogen Occultation Experiment confirmation of
602 stratospheric chlorine decreases in accordance with the Montreal Protocol, *J. Geophys. Res.*, 105, 4483–4490,
603 2000.
- 604 Bernath, P. F.: The Atmospheric Chemistry Experiment (ACE), *J. Quant. Spectrosc. Rad. Transf.*, 186, 3-16,
605 doi:10.1016/j.jqsrt.2016.04.006, 2017.
- 606 Bernath, P., and Fernando, A. M.: Trends in stratospheric HCl from the ACE satellite mission, *Journal of*
607 *Quantitative Spectroscopy and Radiative Transfer*, Volume 217, p. 126-129, doi:10.1016/j.jqsrt.2018.05.027,
608 2018.
- 609 Bernath P. F., Steffen J., Crouse J., and Boone C. D.: Sixteen-year trends in atmospheric trace gases from orbit,
610 *J. Quant. Spectrosc. Rad. Transf.*, 253, doi:10.1016/j.jqsrt.2020.107178, 2020.
- 611 Bernath, P. F., Crouse J., Hughes, R. C., and Boone C. D.: The Atmospheric Chemistry Experiment Fourier
612 Transform Experiment (ACE-FTS) version 4.1 retrievals: Trends and seasonal distributions, *J. Quant.*
613 *Spectrosc. Rad. Transf.*, 259, doi:10.1016/j.jqsrt.2020.107409, 2021.
- 614 Boone, C. D., Bernath, P. F., Cok, D., Jones, S. C., and Steffen, J.: Version 4 retrievals for the Atmospheric
615 Chemistry Experiment Fourier Transform Spectrometer (ACE-FTS) and imagers, *J. Quant. Spectrosc. Radiat.*
616 *Transfer*, 247, doi:10.1016/j.jqsrt.2020.106939, 2020.
- 617 Bourassa, A. E., Degenstein, D. A., Randel, W. J., Zawodny, J. M., Kyrölä, E., McLinden, C. A., Sioris, C. E.,
618 and Roth, C. Z.: Trends in stratospheric ozone derived from merged SAGE II and Odin-OSIRIS satellite
619 observations, *Atmos. Chem. Phys.*, 14, 6983-6994, doi:10.5194/acp-14-6983-2014, 2014.
- 620 Burkholder, J. B., Sander, S. P., Abbatt, J. P. D., Barker, J. R., Huie, R. E., Kolb, C. E., Kurylo, M. J., Orkin, V.
621 L., Wilmouth, D. M., and Wine, P. H.: Chemical kinetics and photochemical data for use in atmospheric
622 studies: Evaluation No. 18, JPL Publication 15-10, Jet Propulsion Laboratory, California Institute of
623 Technology, Pasadena, <http://jpldataeval.jpl.nasa.gov>, 2015.
- 624 Burkholder, J. B., Sander, S. P., Abbatt, J.P.D., Barker, J. R., Cappa, C., Crouse, J. D., Dibble, T. S., Huie, R.
625 E., Kolb, C. E., Kurylo, M. J., Orkin, V. L., Percival, C. J., Wilmouth, D. M., and Wine, P. H.: Chemical
626 kinetics and photochemical data for use in atmospheric studies, Evaluation No. 19, JPL Publication 19-5, Jet
627 Propulsion Laboratory, California Institute of Technology, Pasadena, <http://jpldataeval.jpl.nasa.gov>, 2019.



- 628 Chance, K.V., Johnson, D. G., and Traub, W. A.: Measurement of stratospheric HOCl concentration profiles
629 including diurnal variation, *J. Geophys. Res.*, 94, 11,059-11,069, 1989.
- 630 Coddington, O., Lean, J., Pilewskie, P., Snow, M., and Lindholm, D.: A solar irradiance climate data record, *Bull.*
631 *Amer. Meteor. Soc.*, doi:10.1175/BAMS-D-14-00265.1, 2016.
- 632 Connor, B. J., Mooney, T., Nedoluha, G. E., Barrett, J. W., Par-rish, A., Koda, J., Santee, M. L., and Gomez, R.
633 M.: Re-analysis of ground-based microwave ClO measurements from Mauna Kea, 1992 to early 2012, *Atmos.*
634 *Chem. Phys.*, 13, 8643–8650, doi:10.5194/acp-13-8643-2013, 2013.
- 635 Damiani, A., Funke, B., Marsh, D. R., Lopez-Puertas, M., Santee, M. L., Froidevaux, L., Wang, S., Jackman, C.
636 H., von Clarmann, T., Gardini, A., Cordero, R. R., and Storini, M.: Impact of January 2005 solar proton events
637 on chlorine species, *Atmos. Chem. Phys.*, 12, 4159-4179, doi:10.5194/acp-12-4159-2012, 2012.
- 638 Danabasoglu, G., Lamarque, J.-F., Bacmeister, J., Bailey, D. A., DuVivier, A. K., Edwards, J., Emmons, L. K.,
639 Fasullo, J., Garcia, R., Gettelman, A., Hannay, C., Holland, M. M., Large, W. G., Lauritzen, P. H., Lawrence,
640 D. M., Lenaerts, J. T. M., Lindsay, K., Lipscomb, W. H., Mills, M. J., Neale, R., Oleson, K. W., Otto-
641 Bliesner, B., Phillips, A. S., Sacks, W., Tilmes, S., van Kampenhout, L., Vertenstein, M., Bertini, A.,
642 Dennis, J., Deser, C., Fischer, C., Fox-Kemper, B., Kay, J. E., Kinnison, D. E., Kushner, P. J., Larson, V. E.,
643 Long, M. C., Mickelson, S., Moore, J. K., Nienhouse, E., Polvani, L., Rasch, P. J., and Strand, W. G.: The
644 Community Earth System Model Version 2 (CESM2), *J. Adv. in Modeling Earth Systems*, 12,
645 <https://doi.org/10.1029/2019MS001916>, 2020.
- 646 Efron, B., and Tibshirani, R.: *An Introduction to the Bootstrap*, Monographs on Statistics and Applied Probability
647 57, Chapman and Hall, 1993.
- 648 Emmons, L. K., Schwantes, R. H., Orlando, J. J., Tyndall, G., Kinnison, D., Lamarque, J.-F., Marsh, D., Mills, M.
649 J., Tilmes, S., Bardeen, C., Buchholz, R. R., Conley, A., Gettelman, A., Garcia, R., Simpson, I., Blake, D. R.,
650 Meinardi, S., and Pétron, G.: The Chemistry Mechanism in the Community Earth System Model version 2
651 (CESM2), *Journal of Advances in Modeling Earth Systems*, 12, <https://doi.org/10.1029/2019MS001882>,
652 2020.
- 653 Engel, A., and Rigby, M. (Lead Authors), Burkholder, J. B., Fernandez, R. P., Froidevaux, L., Hall, B. D.,
654 Hossaini, R., Saito, T., Vollmer, M. K., and Yao, B.: Update on Ozone-Depleting Substances (ODSs) and
655 Other Gases of Interest to the Montreal Protocol, Chapter 1 in *Scientific Assessment of Ozone Depletion:*
656 2018, Global Ozone Research and Monitoring Project–Report No. 58, World Meteorological Organization,
657 Geneva, Switzerland, 2018.



- 658 Farman, J., Gardiner, B., and Shanklin, J.: Large losses of total ozone in Antarctica reveal seasonal
659 ClO_x/NO_x interaction, *Nature*, 315, 207–210, doi.org/10.1038/315207a0, 1985.
- 660 Froidevaux, L., Waters, J. W., Read, W. G., Connell, P. S., Kinnison, D. E., and Russell, J. M.: Variations in the
661 free chlorine content of the stratosphere (1991–1997): Anthropogenic, volcanic, and methane influences, *J.*
662 *Geophys. Res.*, 105, D4, 4471–4481, 2000.
- 663 Froidevaux, L., Livesey, N. J., Read, W. G., Salawitch, R. J., Waters, J. W., Drouin, B., MacKenzie, I. A.,
664 Pumphrey, H. C., Bernath, P., Boone, C., Nassar, R., Montzka, S., Elkins, J., Cunnold, D., and Waugh, D.:
665 Temporal decrease in upper atmospheric chlorine, *Geophys. Res. Lett.*, 33, L23813,
666 doi:10.1029/2006GL027600, 2006.
- 667 Froidevaux, L., Kinnison, D. E., Wang, R., Anderson, J., and Fuller, R. A.: Evaluation of CESM1 (WACCM)
668 free-running and specified dynamics atmospheric composition simulations using global multispecies satellite
669 data records, *Atmos. Chem. Phys.*, 19, 4783–4821, doi:10.5194/acp-19-4783-2019, 2019.
- 670 Gelaro, R., McCarty, W., Suarez, M. J., Todling, R., Molod, A., Takacs, L., Randles, C. A., Darmenov,
671 A., Bosilovich, M. G., Reichle, R., Wargan, K., Coy, L., Cullather, R., Draper, C., Akella, S., Buchard,
672 V., Conaty, A., da Silva, A. M., Gu, W., Kim, G.-K., Koster, R., Lucchesi, R., Merkova, D., Nielsen, J.
673 E., Partyka, G., Pawson, S., Putman, W., Rienecker, M., Schubert, S. D., Sienkiewicz, M., and Zhao, B.: The
674 Modern-Era Retrospective Analysis for Research and Applications, Version 2 (MERRA2), *J. Clim.*, 30, 5419–
675 5454, doi:10.1175/JCLI-D-16-0758.1, 2017.
- 676 Gettelman, A., Mills, M. J., Kinnison, D. E., Garcia, R. R., Smith, A. K., Marsh, D. R., Tilmes, S., Vitt, F.,
677 Bardeen, C. G., McInerny, J., Liu, H.-L., Solomon, S. C., Polvani, L. M., Emmons, L. K., Lamarque, J.-F.,
678 Richter, J. H., Glanville, A. S., Bacmeister, J. T., Phillips, A. S., Neale, R. B., Simpson, I. R., DuVivier, A.
679 K., Hodzic, A., and Randel, W. J.: The Whole Atmosphere Community Climate Model version 6 (WACCM6),
680 *J. Geophys. Res.*, 124, 12,380–12,403, doi:10.1029/2019JD030943, 2019.
- 681 Hegglin, M. I., Tegtmeier, S., Anderson, J., Bourassa, A. E., Brohede, S., Degenstein, D., Froidevaux, L., Funke,
682 B., Gille, J., Kasai, Y., Kyrölä, E. T., Lumpe, J., Murtagh, D., Neu, J. L., Pérot, K., Remsberg, E. E., Rozanov,
683 A., Toohey, M., Urban, J., von Clarmann, T., Walker, K. A., Wang, H.-J., Arosio, C., Damadeo, R., Fuller, R.
684 A., Lingenfelter, G., McLinden, C., Pendlebury, D., Roth, C., Ryan, N. J., Sioris, C., Smith, L., and Weigel,
685 K.: Overview and update of the SPARC Data Initiative: comparison of stratospheric composition
686 measurements from satellite limb sounders, *Earth Syst. Sci. Data*, 13, 1855–1903, doi://10.5194/essd-13-1855-
687 2021, 2021.



- 688 Hickson, K. M., Keyser, L. F., and Sander, S. P.: Temperature Dependence of the HO₂ + ClO Reaction. 2. Reaction
689 Kinetics Using the Discharge-Flow Resonance-Fluorescence Technique, *J. Phys. Chem. A*, 111, 8126–8138,
690 2007.
- 691 Jackman, C. H., Marsh, D. R., Vitt, F. M., Garcia, R. R., Fleming, E. L., Labow, G. J., Randall, C. E., Lopez-
692 Puertas, M. L., Funke, B., von Clarmann, T., and Stiller, G. P.: Short- and medium-term atmospheric
693 constituent effects of very large solar proton events, *Atmos. Chem. Phys.*, 8, 765–785, doi:10.5194/acp-8-765-
694 2008, 2008.
- 695 Khosravi, M., Baron, P., Urban, J., Froidevaux, L., Jonsson, A. I., Kasai, Y., Kuribayashi, K., Mitsuda, C.,
696 Murtagh, D. P., Sagawa, H., Santee, M. L., Sato, T. O., Shiotani, M., Suzuki, M., von Clarmann, T., Walker,
697 K. A., and Wang, S.: Diurnal variation of stratospheric and lower mesospheric HOCl, ClO and HO₂ at the
698 equator: comparison of 1-D model calculations with measurements by satellite instruments, *Atmos. Chem.*
699 *Phys.*, 13, 7587-7606, doi:10.5194/acp-13-7587-2013, 2013.
- 700 Kinnison, D. E., Brasseur, G. P., Walters, S., Garcia, R. R., Sassi, F., Boville, B. A., Marsh, D. Harvey, L., Randall,
701 C., Randel, W., Lamarque, J. F., Emmons, L. K., Hess, Orlando, J., Tyndall, G., and Pan, L.: Sensitivity of
702 chemical tracers to meteorological parameters in the MOZART-3 chemical transport model, *J. Geophys. Res.*,
703 112, D20302, doi:10.1029/2006JD007879, 2007.
- 704 Knight, G. P., Beiderhase, T., Helleis, F., Moortgat, G. K., and Crowley, J. N.: Reaction of HO₂ with ClO: Flow
705 Tube Studies of Kinetics and Product Formation between 215 and 298 K, *J. Phys. Chem. A*, 104, 1674–1685,
706 2000.
- 707 Kohlhepp, R., Barthlott, S., Blumenstock, T., Hase, F., Kaiser, I., Raffalski, U., and Ruhnke, R.: Observed and
708 simulated time evolution of HCl, ClONO₂, and HF total column abundances. *Atmos. Chem. Phys.*, 12, 3527–
709 3556, doi:10.5194/acp-11-4669-2011, 2011.
- 710 Kovalenko, L. J., Jucks, K. W., Salawitch, R. J., Toon, G. C., Blavier, J. F., Johnson, D. G., Kleinböhl, A., Livesey,
711 N. J., Margitan, J. J., Pickett, H. M., Santee, M. L., Sen, B., Stachnik, R. A., and Waters, J. W.: Observed and
712 modeled HOCl profiles in the midlatitude stratosphere, Implication for ozone loss, *Geophys. Res. Lett.*, 34,
713 L19801, doi:10.1029/2007GL031100, 2007.
- 714 Kunz, A., Pan, L., Konopka, P., Kinnison, D., and Tilmes, S.: Chemical and dynamical discontinuity at the
715 extratropical tropopause based on START08 and WACCM analysis, *J. Geophys. Res.*, 116, D24302,
716 <https://doi.org/10.1029/2011JD016686>, 2011.



- 717 Kuribayashi, K., Sagawa, H., Lehmann, R., Sato, T. O., and Kasai, Y.: Direct estimation of the rate constant of
718 the reaction $\text{ClO} + \text{HO}_2 \rightarrow \text{HOCl} + \text{O}_2$ from SMILES atmospheric observations. *Atmos. Chem. Phys.*, 14, 255-
719 266, doi:10.5194/acp-14-255-2014, 2014.
- 720 Lamarque, J.-F., Emmons, L. K., Hess, P. G., Kinnison, D. E., Tilmes, S., Vitt, F., Heald, C. L., Holland, E. A.,
721 Lauritzen, P. H., Neu, J., Orlando, J. J., Rasch, P. J., and Tyndall, G. K.: CAM-chem: description and
722 evaluation of interactive atmospheric chemistry in the Community Earth System Model, *Geosci. Model Dev.*,
723 5, 369-411, doi:10.5194/gmd-5-369-2012, 2012.
- 724 Lin, S.-J., A “vertically-Lagrangian” finite-volume dynamical core for global atmospheric models, *Mon.*
725 *Weather Rev.*, 132, 2293–2307, 2004.
- 726 Livesey, N. J., and Read, W. G.: Direct retrieval of line-of-sight atmospheric structure from limb sounding
727 observations, *Geophys. Res. Lett.*, 27, 891-894, doi:10.1029/1999GL010964, 2000.
- 728 Livesey, N. J., Van Snyder, W., Read, W. G., and Wagner, P. A.: Retrieval algorithms for the EOS Microwave
729 Limb Sounder (MLS), *IEEE Trans. Geosci. Remote Sens.*, 44, 1144-1155, doi:10.1109/TGRS.2006.872327,
730 2006.
- 731 Livesey, N. J., Read, W. G., Wagner, P. A., Froidevaux, L., Santee, M. L., Schwartz, M. J., Lambert, A., Manney,
732 G. L., Valle, L. F. M., Pumphrey, H. C., Fuller, R. A., Jarnot, R. F., Knosp, B. W., and Lay, R. R.: EOS MLS
733 Version 5.0x Level 2 and 3 data quality and description document, Tech. rep., Jet Propulsion Laboratory D-
734 105336 Rev. A, available from <https://mls.jpl.nasa.gov/publications>, 2020.
- 735 Livesey, N. J., Read, W. G., Froidevaux, L., Lambert, A., Santee, M. L., Schwartz, M. J., Millán, L. F.,
736 Jarnot, R. F., Wagner, P. A., Hurst, D. F., Walker, K. A., Sheese, P. E., and Nedoluha, G. E.: Investigation
737 and amelioration of long-term instrumental drifts in water vapor and nitrous oxide measurements from the
738 Aura Microwave Limb Sounder (MLS) and their implications for studies of variability and trends, *Atmos.*
739 *Chem. Phys.*, 21, 15409–15430, doi:10.5194/acp-21-15409-2021, 2021.
- 740 Mahieu, E., Chipperfield, M. P., Notholt, J., Reddman, T., Anderson, J., Bernath, P. F., Blumenstock, T., Coffey,
741 M. T., Dhomse, S. S., Feng, W., Franco, B., Froidevaux, L., Griffith, D. W. T., Hannigan, J. W., Hase, F.,
742 Hossaini, R., Jones, N. B., Morino, I., Murata, I., Nakajima, H., Palm, M., Paton-Walsh, C., Russell III, J. M.,
743 Schneider, M., Servais, C., Smale, D., and Walker, K. A.: Recent Northern Hemisphere stratospheric HCl
744 increase due to atmospheric circulation changes, *Nature*, 515, 104-107, doi:10.1038/nature13857, 2014.
- 745 Meinshausen, M., Vogel, E., Nauels, A., Lorbacher, K., Meinshausen, N., Etheridge, D. M., Fraser, P. J., Montzka,
746 S. A., Rayner, P. J., Trudinger, C. M., Krumme, P. B., Beyerle, U., Canadell, J. G., Daniel, J. S., Enting, I. G.,
747 Law, R. M., Lunder, C. R., O’Doherty, S., Prinn, R. G., Reimann, S., Rubino, M., Velders, G. J. M., Vollmer,



- 748 M. K., Wang, R. H.-J., and Weiss, R.: Historical greenhouse gas concentrations for climate modelling
749 (CMIP6), *Geoscientific Model Development*, 10(5), 2057–2116. <https://doi.org/10.5194/gmd-10-2057-2017>,
750 2017.
- 751 Millán, L., Livesey, N., Read, W., Froidevaux, L., Kinnison, D., Harwood, R., MacKenzie, I. A., and Chipperfield,
752 M. P.: New Aura Microwave Limb Sounder observations of BrO and implications for Bry, *Atmos. Meas.*
753 *Tech.*, 5, 1741–1751, doi:10.5194/amt-5-1741-2012, 2012.
- 754 Millán, L. F., Wang, S., Livesey, N., Kinnison, D., Sagawa, H., and Kasai, Y.: Stratospheric and mesospheric
755 HO₂ observations from the Aura Microwave Limb Sounder, *Atmos. Chem. Phys.*, 15, 2889–2902,
756 doi:10.5194/acp-15-2889-2015, 2015.
- 757 Millán, L. F., Livesey, N. J., Santee, M. L., Jessica L. Neu, J. L., Manney, G. L., and Fuller, R. A.: Case studies
758 of the impact of orbital sampling on stratospheric trend detection and derivation of tropical vertical velocities:
759 solar occultation vs. limb emission sounding, *Atmos. Chem. Phys.*, 16, 11521–11534,
760 <https://doi.org/10.5194/acp-16-11521-2016>, 2016.
- 761 Molina, M. J., and Rowland, F. S.: Stratospheric sink for chlorofluoro-methanes: Chlorine atom catalysed
762 destruction of ozone, *Nature*, 249, 810–812, 1974.
- 763 Montzka, S. A., Dutton, G. S., Yu, P., Ray, E., Portmann, R. W., Daniel, J. S., Kuijpers, L., Hall, B. D., Mondeel,
764 D., Siso, C., Nance, J. D., Rigby, M., Manning, A. J., Hu, L., Moore, F., Miller, B. R., and Elkins, J. W. : An
765 unexpected and persistent increase in global emissions of ozone-depleting CFC-11, *Nature*, 557(7705), 413-
766 417, doi:10.1038/s41586-018-0106-2, 2018.
- 767 Morgenstern, O., Hegglin, M. I., Rozanov, E., O’Connor, F. M., Abraham, N. L., Akiyoshi, H., Archibald, A. T.,
768 Bekki, S., Butchart, N., Chipperfield, M. P., Deushi, M., Dhomse, S. S., Garcia, R. R., Hardiman, S. C.,
769 Horowitz, L. W., Joeckel, P., Josse, B., Kinnison, D., Lin, M., Mancini, E., Manyin, M. E., Marchand, M.,
770 Marecal, V., Michou, M., Oman, L. D., Pitari, G., Plummer, D. A., Revell, L. E., Saint-Martin, D., Schofield,
771 R., Stenke, A., Stone, K., Sudo, K., Tanaka, T. Y., Tilmes, S., Yamashita, Y., Yoshida, K., and Zeng, G.:
772 Review of the global models used within phase 1 of the Chemistry-Climate Model Initiative (CCMI), *Geosci.*
773 *Model Dev.*, 10, 639–671, <https://doi.org/10.5194/gmd-10-639-2017>, 2017.
- 774 Nassar, R., Bernath, P. F., Boone, C. D., Clerbaux, C., Coheur, P. F., Dufour, G., Froidevaux, L., Mahieu, E.,
775 McConnell, J. C., McLeod, S. D., Murtagh, D. P., Rinsland, C. P., Semeniuk, K., Skelton, R., Walker, K. A.,
776 and Zander, R.: A global inventory of stratospheric chlorine in 2004, *J. Geophys. Res.*, 111, D22312,
777 doi:10.1029/2006JD007073, 2006.



- 778 Neely, R. R., and Schmidt, A.: “VolcanEESM: Global volcanic sulphur dioxide (SO₂) emissions database from
779 1850 to present - Version 1.0.”, <https://doi.org/10.5285/76ebdc0b-0eed-4f70-b89e-55e606bcd568>, 2016.
- 780 Nedoluha, G., Connor, B. J., Mooney, T., Barrett, J. W., Parrish, A., Gomez, R. M., Boyd, I., Allen, D. R.,
781 Kotkamp, M., Kremser, S., Deshler, T., Newman, P., and Santee, M. L.: 20 years of ClO measurements in the
782 Antarctic lower stratosphere, *Atmos. Chem. Phys.*, 16, 10725–10734, doi:10.5194/acp-16-10725-2016, 2016.
- 783 Nickolaisen, S. L., Roehl, C. M., Blakeley, L. K., Friedl, R. R., Francisco, J. S., Liu, R., and Sander, S. P.:
784 Temperature Dependence of the HO₂ + ClO Reaction. 1. Reaction Kinetics by Pulsed Photolysis-Ultraviolet
785 Absorption and ab Initio Studies of the Potential Surface, *J. Phys. Chem. A*, 104, 308–319, 2000.
- 786 O’Doherty, S., Cunnold, D. M., Manning, A., Miller, B. R., Wang, R. H.-J., Krummel, P. B., Fraser, P. J.,
787 Simmonds, P. G., McCulloch, A., Weiss, R. F., Salameh, P., Porter, L. W., Prinn, R. G., Huang, J., Sturrock,
788 G., Ryall, D., Derwent, R. G., and Montzka, S. A.: Rapid growth of hydrofluorocarbon 134a and
789 hydrochlorofluorocarbons 141b, 142b, and 22 from Advanced Global Atmospheric Gases Experiment
790 (AGAGE) observations at Cape Grim, Tasmania, and Mace Head, Ireland, *J. Geophys. Res.*, 109, D06310,
791 doi:10.1029/2003JD004277, 2004.
- 792 O’Neill, B. C., Tebaldi, C., van Vuuren, D. P., Eyring, V., Friedlingstein, P., Hurtt, G., Knutti, R., Kriegler, E.,
793 Lamarque, J.-F., Lowe, J., Meehl, G. A., Moss, R., Riahi, K., and Sanderson, B. M.: The Scenario Model
794 Intercomparison Project (Scenario MIP) for CMIP6, *Geosci. Model Dev.*, 9, 3461–3482,
795 <https://gmd.copernicus.org/articles/9/3461/2016/doi:10.5194/gmd-9-3461-2016>, 2016.
- 796 Randel, W. J., and Thompson, A. M.: Interannual variability and trends in tropical ozone derived from SAGE II
797 satellite data and SHADOZ ozonesondes, *J. Geophys. Res.*, 116, D07303, doi:10.1029/2010JD015195, 2011.
- 798 Read, W. G., Shippony, Z., and Snyder, W. V.: The clear-sky unpolarized forward model for the EOS Aura
799 microwave limb sounder (MLS), *IEEE Trans. Geosci. Remote Sens.*, 44, 1367-1379,
800 doi://10.1109/TGRS.2006.862267, 2006.
- 801 Riahi, K., van Vuuren, D. P., Kriegler, E., Edmonds, J., O’Neill, B. C., Fujimori, S., Bauer, N., Calvin, K., Dellink,
802 R., Fricko, O., Lutz, W., Popp, A., Crespo Cuaresma, J., Samir, K. C., Leimbach, M., Jiang, L., Kram, T., Rao,
803 S., Emmerling, J., Ebi, K., Hasegawa, T., Havlik, P., Humpenöder, F., Aleluia Da Silva, L., Smith, S., Stehfest,
804 E., Bosetti, V., Eom, J., Gernaat, D., Masui, T., Rogelj, J., Strefler, J., Drouet, L., Krey, V., Luderer, G.,
805 Harmsen, M., Takahashi, K., Baumstark, L., Doelman, J. C., Kainuma, M., Klimont, Z., Marangoni, G., Lotze-
806 Campen, H., Obersteiner, M., Tabeau, A., Tavoni, M.: The Shared Socioeconomic Pathways and their energy,
807 land use, and greenhouse gas emissions implications: An overview, *Global Environ. Chang.*, 42, 1045 153–
808 168, <https://doi.org/10.1016/j.gloenvcha.2016.05.009>, 2017.



- 809 Rodgers, C.: Inverse Methods for Atmospheric Sounding: Theory and Practice, Vol. 2 of Series on Atmospheric,
810 Oceanic and Planetary Physics, World Scientific, Singapore, 2000.
- 811 Sander, S. P., Finlayson-Pitts, B. J., Friedl, R. R., Golden, D. M., Huie, R. E., Keller-Rudek, H., Kolb, C. E.,
812 Kurylo, M. J., Molina, M. J., Moortgat, G. K., Orkin, V. L., Ravishankara, A. R., and Wine, P. H.: Chemical
813 Kinetics and Photochemical Data for Use in Atmospheric Studies, Evaluation Number 15, JPL Publication
814 06-2, Jet Propulsion Laboratory, California Institute of Technology, Pasadena, 2006.
- 815 Siskind, D. E., Froidevaux, L., Russell, J. M., and Lean, J.: Implications of upper stratospheric trace constituent
816 changes observed by HALOE for O₃ and ClO from 1992 to 1995, *Geophys. Res. Lett.*, 25, 18, 3513-3516,
817 doi:10.1029/98GL02664, 1998.
- 818 Solomon, P., Barrett, J., Mooney, T., Connor, B., Parrish, A., and Siskind, D. E.: Rise and decline of active
819 chlorine in the stratosphere, *Geophys. Res. Lett.*, 33, L18807, doi:10.1029/2006GL027029, 2006.
- 820 Solomon, S., and Garcia, R. R.: On the distribution of long-lived tracers and chlorine species in the middle
821 atmosphere, *J. Geophys. Res.*, 89, D7, 11,633–11,644, 1984.
- 822 SPARC: The SPARC Data Initiative: Assessment of stratospheric trace gas and aerosol climatologies from
823 satellite limb sounders, M. I. Hegglin and S. Tegtmeier (eds.), SPARC Report No. 8, WCRP-5/2017, available
824 at www.sparc-climate.org/publications/sparc-reports/, 2017.
- 825 Steiner, A. K., Ladstädter, F., Randel, W. J., Maycock, A. C., Fu, Q., Claud, C., Gleisner, H., Haimberger, L., Ho,
826 S.-P., Keckhut, P., Leblanc, T., Mears, C., Polvani, L. M., Santer, B. D., Schmidt, T., Sofieva, V., Wing, R.,
827 and Zou, C.-Z.: Observed Temperature Changes in the Troposphere and Stratosphere from 1979 to 2018,
828 doi:10.1175/JCLI-D-19-0998.1, 2021.
- 829 Stimpfle, R., Perry, R., and Howard, C. J.: Temperature dependence of the reaction of ClO and HO₂ radicals, *J.*
830 *Chem. Phys.*, 71, 5183–5190, doi:10.1063/1.438293, 1979.
- 831 Strahan, S. E., Smale, D., Douglass, A.R., Blumenstock, T., Hannigan, J. W., Hase, F., Jones, N. B., Mahieu, E.,
832 Notholt, J., Oman, L. D., Ortega, I., Palm, M., Prignon, M., Robinson, J., Schneider, M., Sussmann, R., and
833 Velasco, V. A.: Observed hemispheric asymmetry in stratospheric transport trends from 1994 to 2018,
834 *Geophys. Res. Lett.*, 47, e2020GL088567, doi:10.1029/2020GL088567, 2020.
- 835 Tapping, K.F.: The 10.7 cm solar radio flux (F10.7), *Space Weather*, 11, 394-406, doi:10.1002/swe.20064, 2013.
- 836 Tiao, G. C., Reinsel, G. C., Xu, D., Pedrick, J. H., Zhu, X., Miller, A. J., DeLuisi, J. J., Mateer, C. L., and Wuebbles,
837 D. J.: Effects of autocorrelation and temporal sampling schemes on estimates of trend and spatial correlation,
838 *J. Geophys. Res.*, 95, 20507–20517, doi:10.1029/JD095iD12p20507, 1990.



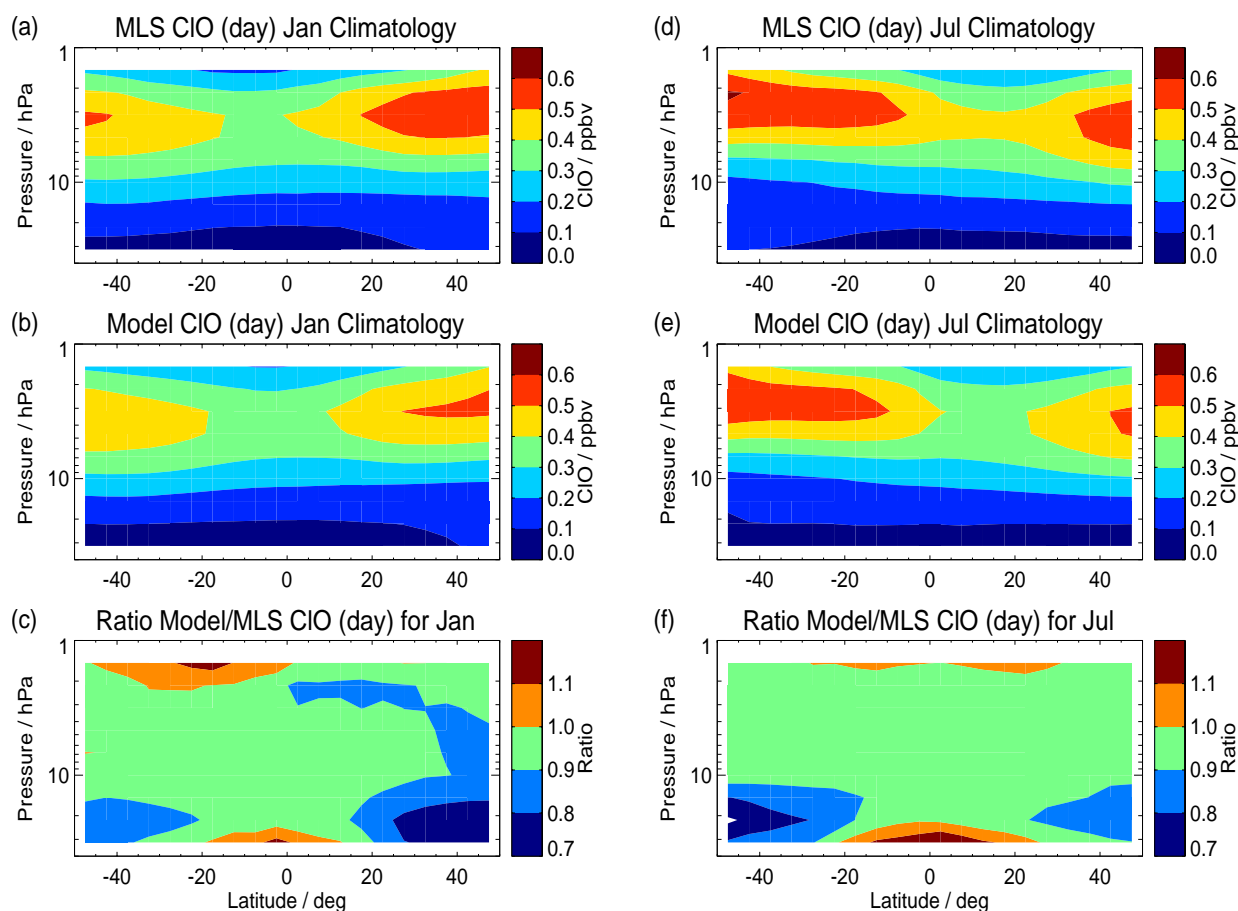
- 839 Tilmes, S., Hodzic, A., Emmons, L. K., Mills, M. J., Gettelman, A., Kinnison, D. E., Park, M., Lamarque, J.-F.,
840 Vitt, F., Shrivastava, M., Campuzano-Jost, P., Jimenez, J. L., and Liu, X.: Climate forcing and trends of
841 organic aerosols in the Community Earth System Model (CESM2), *J. of Adv. in Modeling Earth Systems*, 11,
842 4323–4351, doi:10.1029/2019MS001827, 2019.
- 843 von Clarmann, T., Glatthor, N., Grabowski, U., Höpfner, M., Kellmann, S., Linden, A., Mengistu Tsidu, G., Milz,
844 M., Steck, T., Stiller, G. P., Fischer, H., and Funke, B.: Global stratospheric HOCl distributions retrieved from
845 infrared limb emission spectra recorded by the Michelson Interferometer for Passive Atmospheric Sounding
846 (MIPAS), *J. Geophys. Res.*, 111, D05311, doi:10.1029/2005JD005939, 2006.
- 847 von Clarmann, T., Glatthor, N., Ruhnke, R., Stiller, G. P., Kirner, O., Reddman, T., Höpfner, M., Kellmann, S.,
848 Kouker, W., Linden, A., and Funke, B.: HOCl chemistry in the Antarctic Stratospheric Vortex 2002, as
849 observed with the Michelson Interferometer for Passive Atmospheric Sounding (MIPAS), *Atmos. Chem.*
850 *Phys.*, 9, 1817–1829, doi:10.5194/acp-9-1817-2009, 2009.
- 851 von Clarmann, T., Funke, B., Glatthor, N., Kellmann, S., Kiefer, M., Kirner, O., Sinnhuber, B.-M., and Stiller, G.
852 P.: The MIPAS HOCl climatology, *Atmos. Chem. Phys.*, 12, 1965–1977, doi:10.5194/acp-12-1965-2012,
853 2012.
- 854 Ward, M. K. M. and Rowley, D. M.: Kinetics of the ClO + CH₃O₂ reaction over the temperature range T=250–
855 298 K, *Phys. Chem. Chem. Phys.*, 18, 13,646–13,656, doi:10.1039/c6cp00724d, 2016.
- 856 Waters, J. W., Hardy, J. C., Jarnot, R. F., and H. M. Pickett, H. M.: Chlorine monoxide radical, ozone, and
857 hydrogen peroxide: Stratospheric measurements by microwave limb sounding. *Science*, 214, 61–64, doi:
858 10.1126/science.214.4516.61, 1981.
- 859 Waters, J., Froidevaux, L., Harwood, R., Jarnot, R., Pickett, H., Read, W., Siegel, P., Cofield, R., Filipiak, M.,
860 Flower, D., Holden, J., Lau, G., Livesey, N., Manney, G., Pumphrey, H., Santee, M., Wu, D., Cuddy, D., Lay,
861 R., Loo, M., Perun, V., Schwartz, M., Stek, P., Thurstans, R., Boyles, M., Chandra, S., Chavez, M., Chen, G.-
862 S., Chudasama, B., Dodge, R., Fuller, R., Girard, M., Jiang, J., Jiang, Y., Knosp, B., LaBelle, R., Lam, J., Lee,
863 K., Miller, D., Oswald, J., Patel, N., Pukala, D., Quintero, O., Scaff, D., Snyder, V., Tope, M., Wagner, P.,
864 and Walch, M.: The Earth Observing System Microwave Limb Sounder (EOS MLS) on the Aura satellite,
865 *IEEE Transac. Geosci. Remote Sens.*, 44, 5, doi:10.1109/TGRS.2006.873771, 2006.
- 866 Waugh, D. W., Considine, D. B., and Fleming, E. L.: Is upper stratospheric chlorine decreasing as expected?,
867 *Geophys. Res. Lett.*, 28, 1187–1190, <https://doi.org/10.1029/2000GL011745>, 2001.
- 868 Weatherhead, E. C., Reinsel, G. C., Tiao, G. C., Meng, X. L., Choi, D., Cheang, W. K., Keller, T., DeLuisi, J.,
869 Wuebbles, D. J., Kerr, J. B., Miller, A. J., Oltmans, S. J., and Frederick J. E.: Factors affecting the detection



870 of trends: Statistical considerations and applications to environmental data, *J. Geophys. Res.*, 103, 17149–
871 17161, doi:10.1029/98JD00995, 1998.

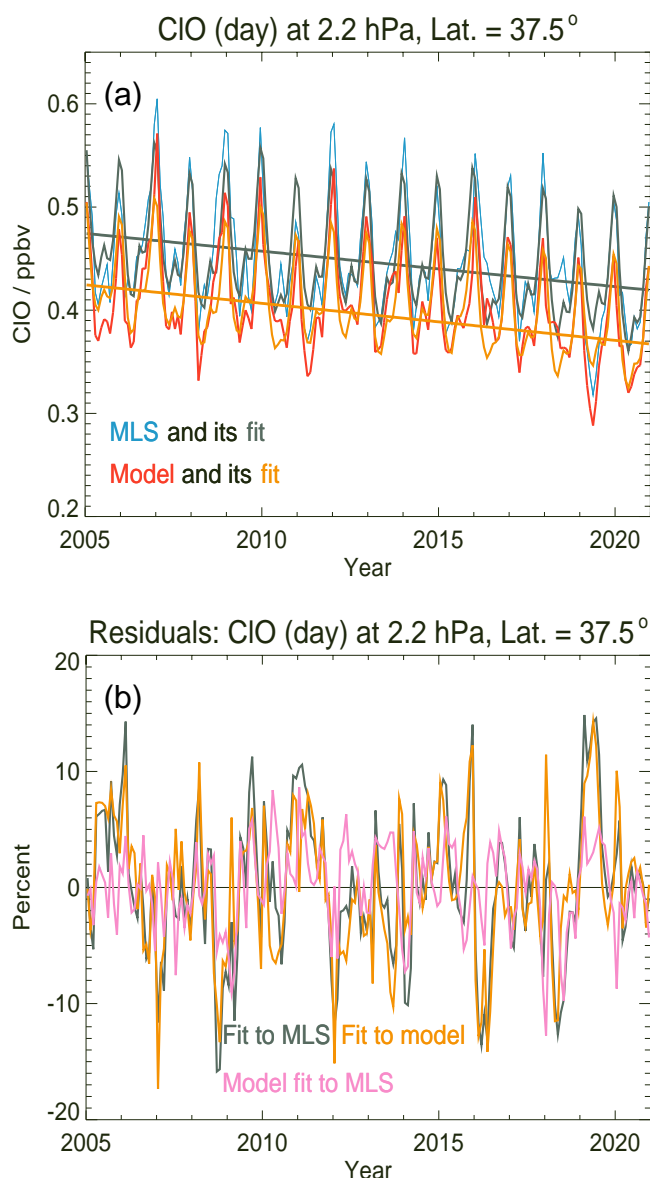
872 WMO: Scientific assessment of ozone depletion: 2018, Global Ozone Research and Monitoring Project–Report
873 No. 58, Geneva, Switzerland, 2018.

874 Zander, R., Gunson, M. R., Farmer, C. B., Rinsland, C. P., Irion, F. W., and Mahieu, E.: The 1985 chlorine and
875 fluorine inventories in the stratosphere based on ATMOS observations at 30° north latitude, *J. Atmos. Chem.*,
876 15, 171-186, <https://doi.org/10.1007/BF00053758>, 1992.



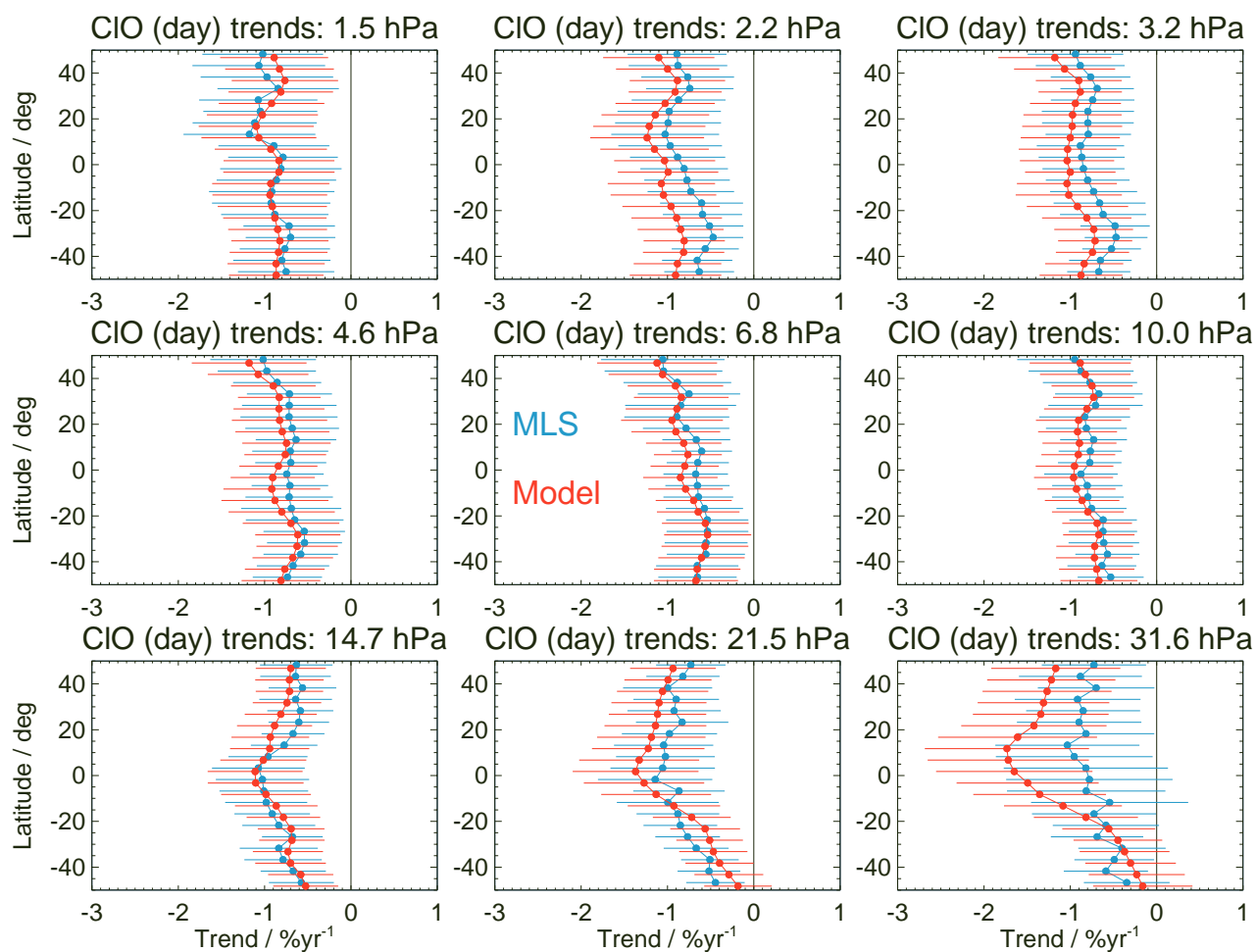
877
878

879 **Figure 1.** Climatological mean fields (over 2005 through 2020 for CIO (daytime data) from MLS and model results between
880 50°S and 50°N and 32 to 1.5 hPa. Daytime averages (observed and simulated values) are based on values with solar zenith
881 angles less than 90° only. (a) and (b) show the January MLS and model climatologies, respectively, while (c) gives the ratio
882 (model values divided by MLS values) for that month; (d), (e), and (f) are the same as (a), (b), and (c), respectively, but for
883 July instead of January. The model daily values (throughout this work) were sampled to provide the closest match in space
884 and time to the MLS daily Level 2 data; model results were then binned in latitude and averaged over each month, and
885 interpolated to the MLS pressure grid, in order to best match the averaging process of MLS monthly zonal mean data.



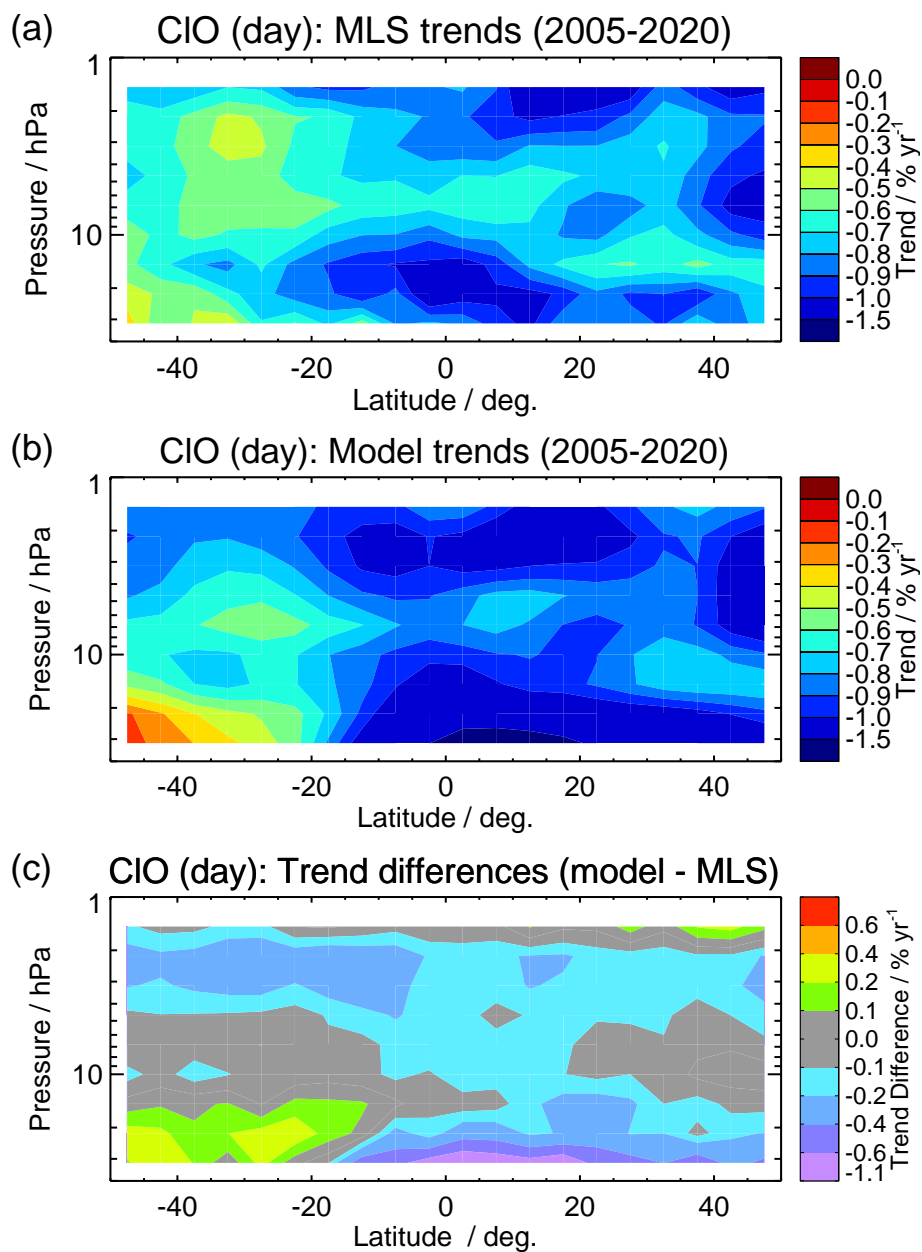
886
887

888 **Figure 2.** (a) Examples of MLS and model CIO (day) monthly zonal mean time series (2005 through 2020) for the 35°N–
889 40°N latitude bin at 2.2 hPa. The MLS data (blue) are fitted by a regression model (grey), and the model series (red) is fitted
890 by the same type of regression model (orange). The grey and orange lines are the linear components of the corresponding fits
891 to the MLS and model curves, respectively. (b) Residuals, with the fit to MLS (minus MLS) in grey, the fit to the model (minus
892 the model) in orange, and the de-biased model fit to MLS (minus MLS) in pink.



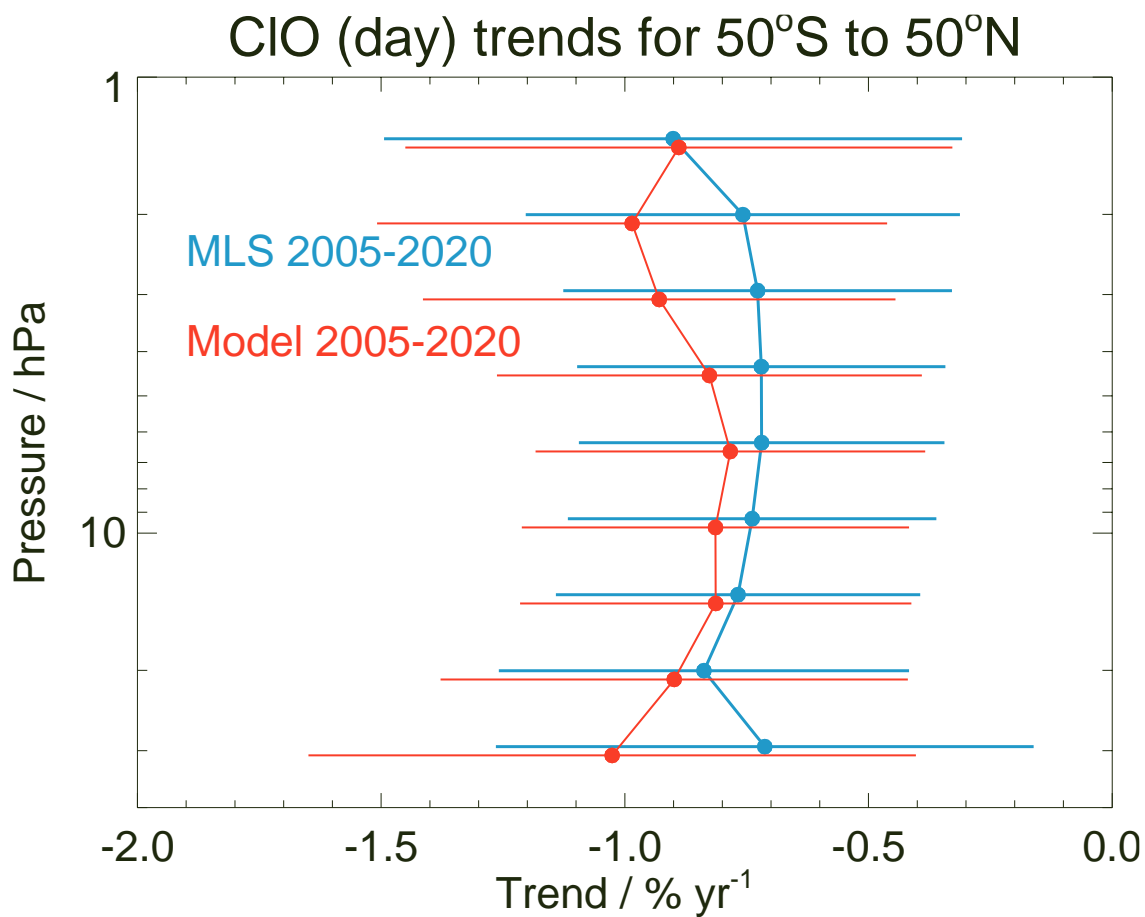
893
894
895
896
897
898

Figure 3. Linear trends in upper stratospheric CIO (2005 through 2020) at different pressure levels versus latitude, as obtained from multiple regression analyses applied to monthly zonal mean daytime series from MLS (blue) and the model (red). Error bars depict the uncertainties (2σ) for these trend results, based on block bootstrap analyses of the monthly residual series from the fits to the MLS and model series.



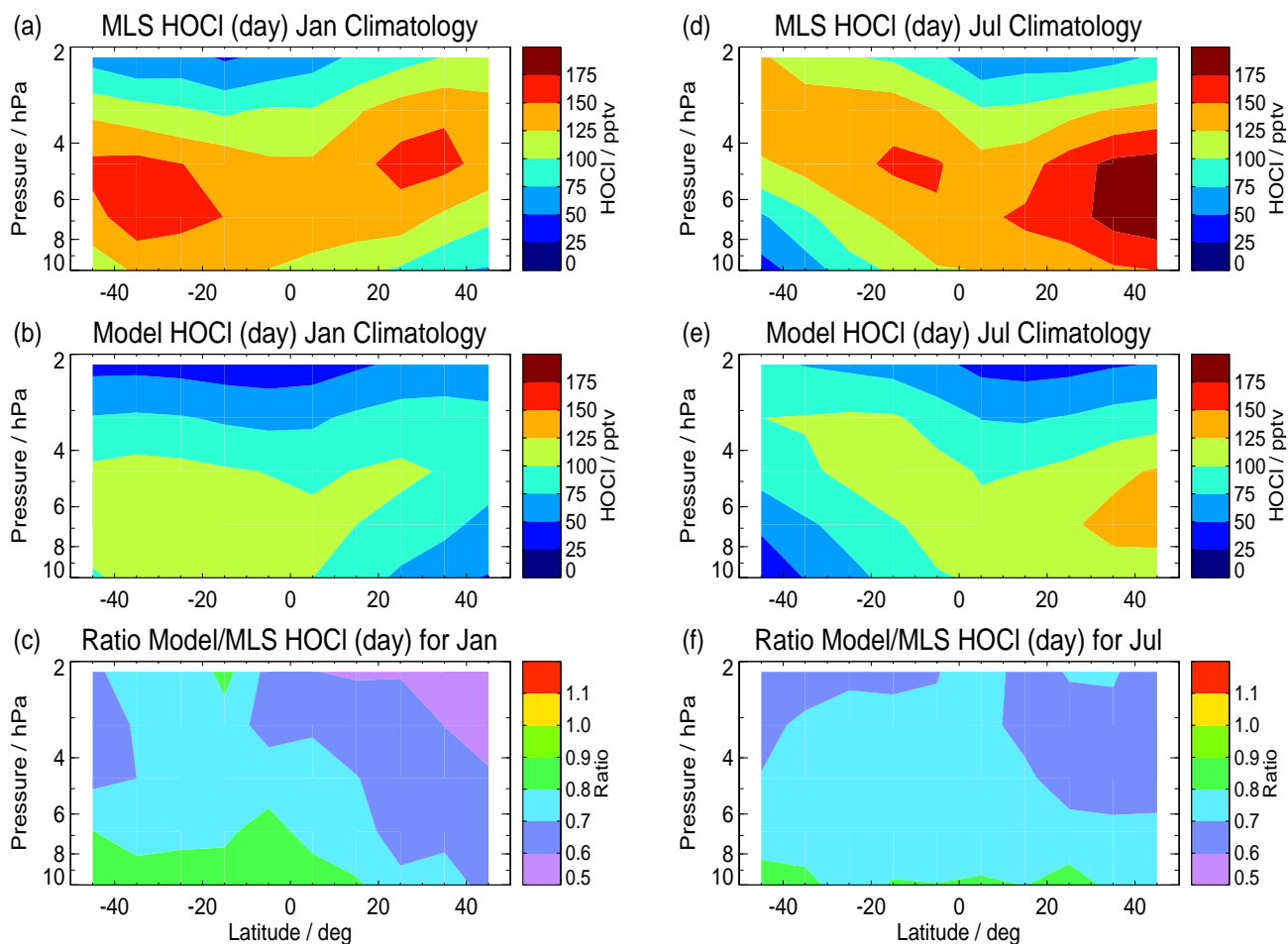
899
900
901
902

Figure 4. Contour plots of CIO (day) trends ($\% \text{yr}^{-1}$) for the period 2005 through 2020 from (a) MLS, and (b) model, with (c) showing the differences ($\% \text{yr}^{-1}$) in these trends (model – MLS).



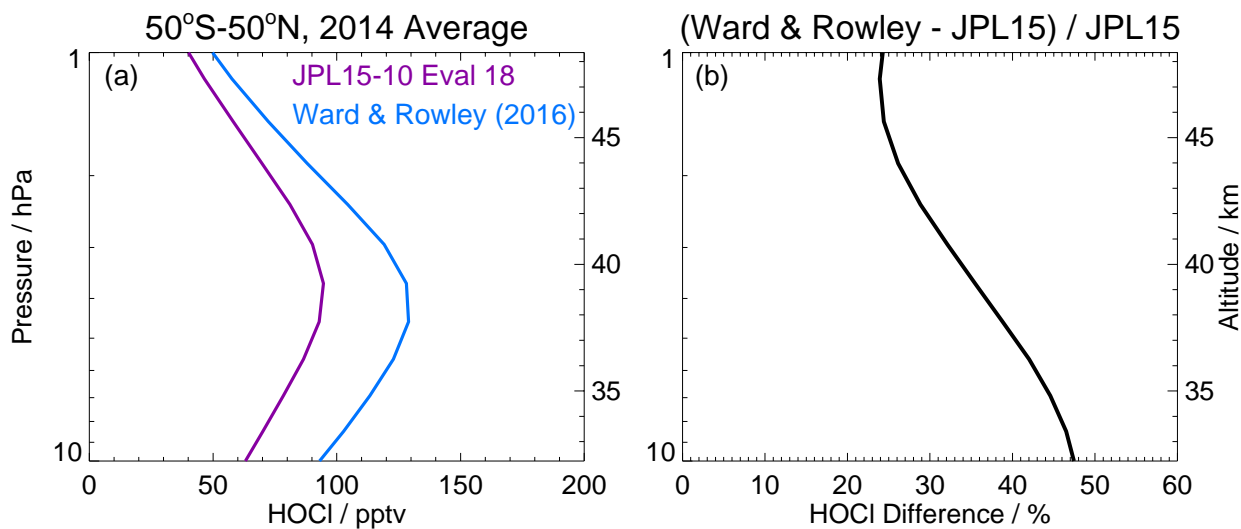
903
904
905
906
907

Figure 5. Trends in CIO (daytime values) over 2005 through 2020 from MLS (blue) and model (red) for the 50°S to 50°N latitude range. Error bars depict the uncertainties (2σ) for these trend results, based on block bootstrap analyses of the monthly residual series from the fits to the MLS and model time series.



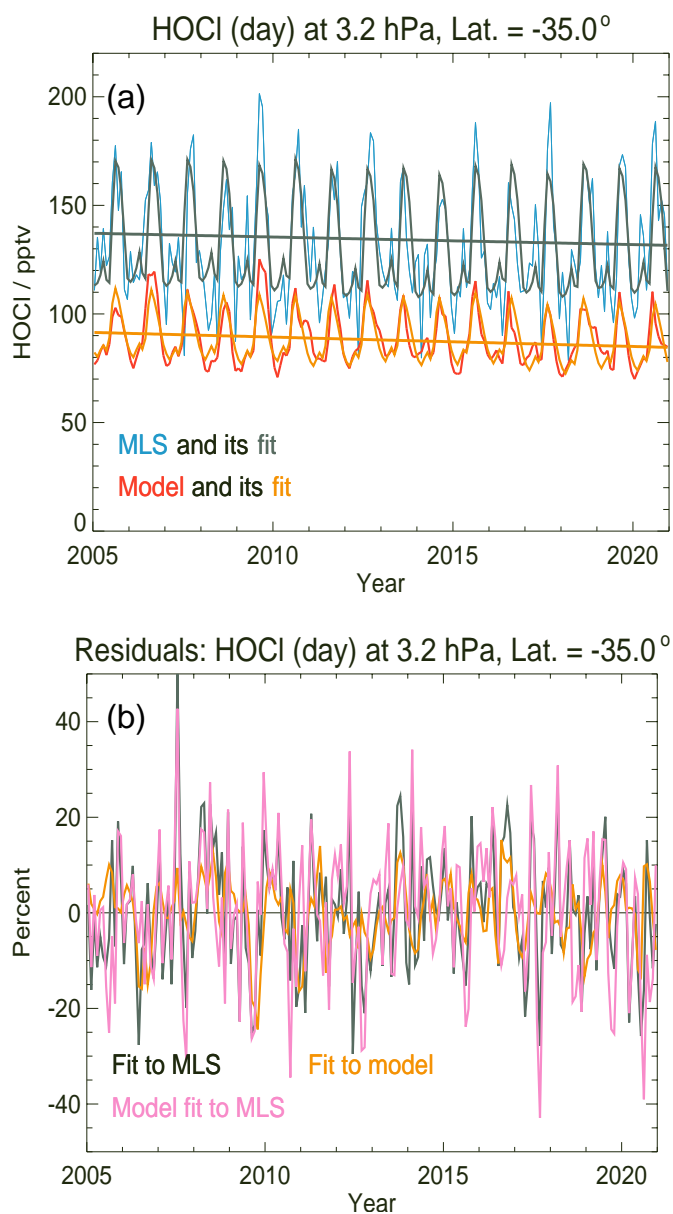
908
909
910
911
912

Figure 6. Same as Figure 1, except for climatological (2005–2020) HOCl daytime values from MLS and the model (see text for more details); the vertical range for useful MLS HOCl data (and for related trend analyses) is 10 to 2.2 hPa.



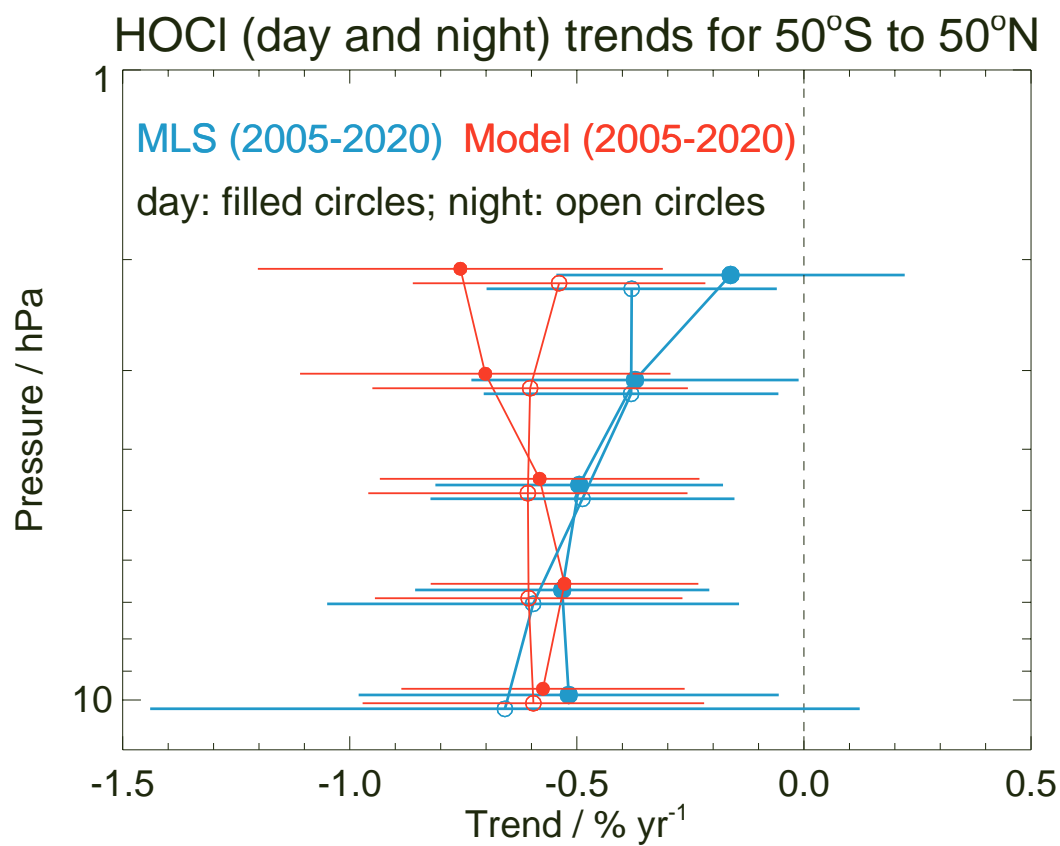
913
914

915 **Figure 7.** (a) Sensitivity of average (for 2014, 50°S to 50°N) model upper stratospheric HOCl profile (pptv) to the choice of
916 rate constant for the HOCl formation reaction between HO₂ and ClO. The JPL 15-10 Evaluation 18 rate constant choice gives
917 the purple average profile, whereas the larger rate constant derived by Ward and Rowley (2016) leads to the blue average
918 profile. (b) The percent difference (increase) between the two curves in panel (a) (blue minus purple).



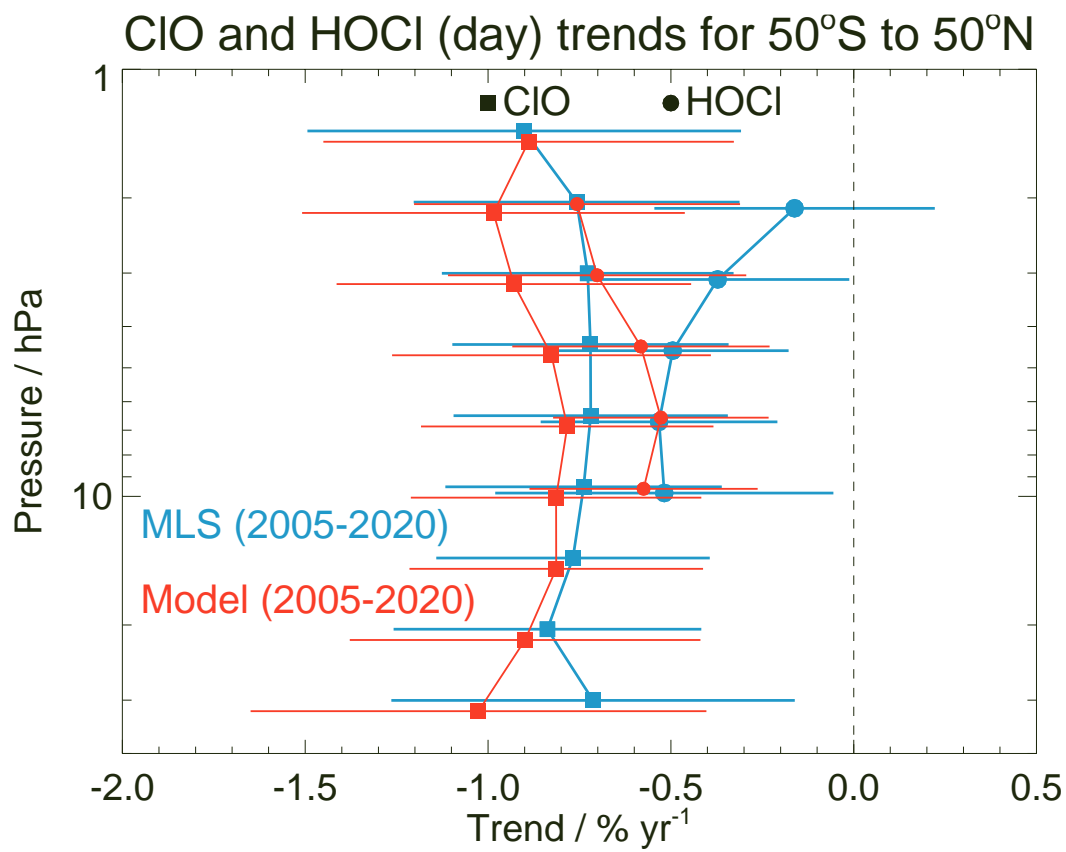
919
920
921
922

Figure 8. Same as Fig. 2, except for an example of (a) HOCl time series and regression fits and (b) residuals for 3.2 hPa and the 30°S to 40°S latitude bin.



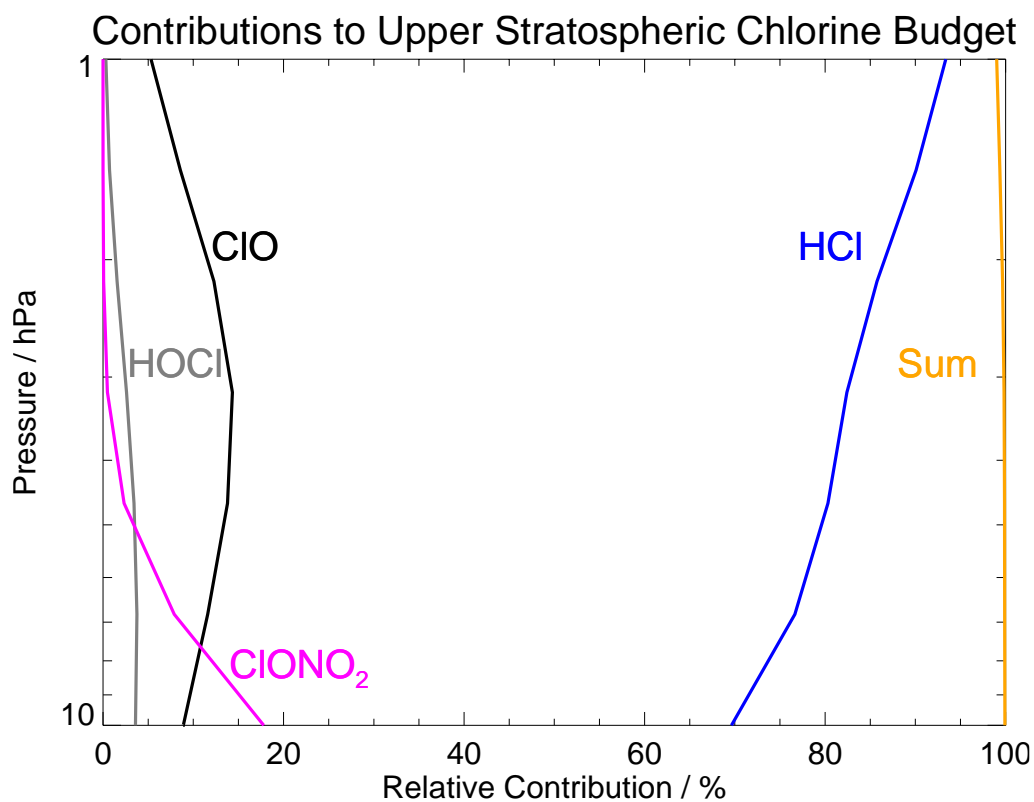
923
924
925
926

Figure 9. Same as Fig. 5, except for trend results for HOCl from both day (filled circles) and night (open circles) time series analyses between 10 and 2.2 hPa.



927
928
929
930
931

Figure 10. Derived upper stratospheric trends in ClO (filled squares) and HOCl (filled circles) based on regression fits to daytime monthly zonal mean time series for both species, for 50°S to 50°N averages from 2005 through 2020; MLS results are in blue and model results in red.

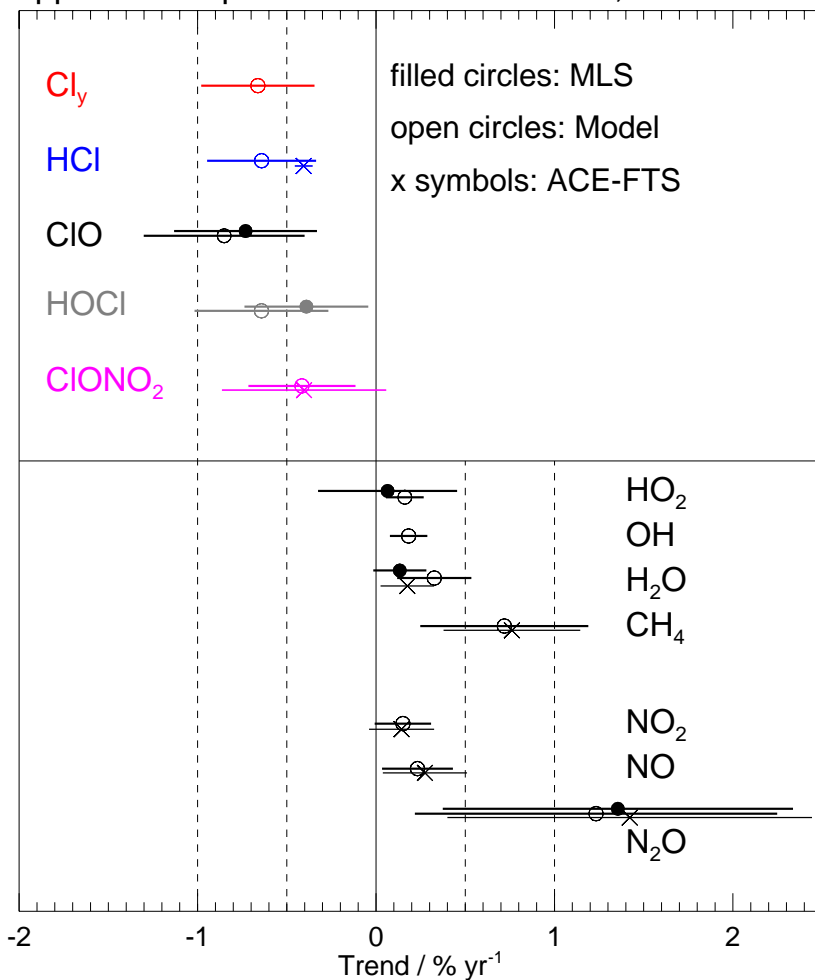


932
933
934
935
936
937

Figure 11. Percent contributions of various species (daytime HCl, ClO, HOCl, and ClONO₂) to the upper stratospheric chlorine budget between 10 and 1 hPa, based on climatological (16-yr) daytime model results in the 50°S to 50°N latitude range. The sum of these contributions is shown in orange; there are also very small contributions in this pressure range from other species (Cl, Cl₂, Cl₂O₂, OClO, BrCl, which are not represented here).



Upper Stratospheric Trends: 2005-2020, 50°S to 50°N



938
939

940 **Figure 12.** Upper stratospheric trends in various species from 6.8 to 2.2 hPa for 50°S to 50°N, based on linear trends obtained
941 from the regression fits to daytime time series of MLS data (filled circles) and/or model series (open circles); x symbols are
942 from our analysis of (50°S to 50°N) ACE-FTS version 4.1 data over the 33 to 43 km range (see text). Error bars represent
943 uncertainties (2σ), derived as described in the text.